2018-07-01

Use of Phase and Amplitude Gradient Estimation for Acoustic Source Characterization and Localization

Joseph Scott Lawrence
Brigham Young University

Use of Phase and Amplitude Gradient Estimation for Acoustic Source Characterization and Localization

Joseph Scott Lawrence

A thesis submitted to the faculty of
Brigham Young University
in partial fulfillment of the requirements for the degree of

Master of Science

Kent L. Gee, Chair
Tracianne B. Neilsen
Scott D. Sommerfeldt

Department of Physics and Astronomy

Brigham Young University

ABSTRACT

Use of Phase and Amplitude Gradient Estimation for Acoustic Source Characterization and Localization

Joseph Scott Lawrence
Department of Physics and Astronomy, BYU
Master of Science

Energy-based acoustic quantities provide vital information about acoustic fields and the characterization of acoustic sources. Recently, the phase and amplitude gradient estimator (PAGE) method has been developed to reduce error and extend bandwidth of energy-based quantity estimates. To inform uses and applications of the method, analytical and experimental characterizations of the method are presented. Analytical PAGE method bias errors are compared with those of traditional estimation for two- and three-microphone one-dimensional probes. For a monopole field when phase unwrapping is possible, zero bias error is achieved for active intensity using three-microphone PAGE and for specific acoustic impedance using two-microphone PAGE. A method for higher-order estimation in reactive fields is developed, and it is shown that a higher-order traditional method outperforms higher-order PAGE for reactive intensity in a standing wave field. Extending the applications of PAGE, the unwrapped phase gradient is used to develop a method for directional sensing with improved bandwidth and arbitrary array response.

Keywords: acoustic intensity, reactive intensity, specific acoustic impedance, directional pressure, bandwidth extension

ACKNOWLEDGENTS

It has been such a privilege to study acoustics at BYU. And what a journey it's been! So many people have helped me along the way, and though I cannot thank everyone by name, I am immeasurably grateful for all the assistance I've received and the friendships I've gained.

A huge thank you goes to Dr. Gee. Even before he was my advisor, his guidance and his stellar teaching of my first acoustics classes were instrumental in my decision to join the program for graduate school. I'm especially grateful for his encouragement to publish throughout my time here. This has improved the quality of my research and made the thesis-writing process very efficient. His guidance, passion for acoustics, and strength of character have made a great positive impact on my life.

I'm also grateful for the other acoustics faculty who have helped me along the way. Dr. Sommerfeldt has provided knowledge and wisdom in my research topics and in class. In addition to teaching me "magimatics," he instilled in me a desire to live the mission of BYU, and a commitment to attend campus devotionals, which provided an education for character and spirit that I'm very grateful for. Dr. Neilsen has consistently provided substantial knowledge and good advice about both research and life. Her tips on writing and presenting have been instrumental in being able to effectively share my research. Also, Dr. Anderson and Dr. Leishman both taught great classes and have been impactful examples for me.

A special thanks goes out to my great friends Sarah Young, Kelli Succo, and Brian Patchett. Each of them have helped make our somewhat-drab office into a special place. All the questions answered, support given, jokes shared, and stories told have really meant a lot. I'm also grateful for the assistance and friendship of my other fellow students: Mylan Cook, Kevin Leete, Michael Denison, Travis Hoyt, Pegah Aslani, Brent Reichman, Blaine Harker, Hales Swift, Caleb Goates,

Michael Rose, Nathaniel Wells, Reese Rasband, Jacey Young, Daxton Hawks, Michael Mortenson, and David Van Komen. Additionally, I'm very thankful for Eric Whiting for providing such a solid foundation upon which my research is primarily built.

The constant love and support from my family means the world to me. Thank you to my parents for teaching me so much and for inspiring me to go far. I'm also grateful for my siblings, who are each wonderful friends and examples to me. Finally, a thank you goes out to all the people who have acted as members of my surrogate family, supporting me as I've been away from home. In particular, my long-time roommate Nick Mena has been a dear friend and a great support through everything.

If I missed anyone (and I'm sure I did), thanks to you too! None of this could have been done alone, and all the support means a lot.

Lastly, a special thank you to the National Science Foundation and to the BYU Department of Physics and Astronomy for funding this research, making all this possible.

Table of Contents

List of Figures

List of Tables:

Chapter 1

Introduction

1.1 Motivation

Estimation of energy-based acoustical quantities provides information used in the characterization and localization of acoustic sources. These estimates rely on both the acoustic pressure, a scalar quantity measured with a microphone, and the acoustic particle velocity, a vector quantity often estimated using microphone arrays. Some energy-based quantities include active intensity, reactive intensity, and specific acoustic impedance, each of which are discussed in this thesis.

An energy-based quantity of particular importance is active intensity, which represents the amount of propagating acoustic energy per unit area in the field. Active intensity is a vector quantity that points in the direction of propagation, and can be used in source localization[1] or holography.[2-4] Additionally, through integration of active intensity the sound power of an acoustic source can be estimated.[5-7] Unlike field quantities such as pressure and particle velocity, sound power is a source property, providing information about the source itself. Knowledge of sound power and location of a source can inform efforts in noise control, source detection, and source characterization.

A method for estimation of active intensity was developed in the 1970s.[8-11] This method is still in use today and is referred to as the traditional method throughout the current work. A traditional one-dimensional intensity probe consists of two microphones, with center pressure

estimated using the pressure sum to obtain the average. The center particle velocity is estimated using the pressure difference and Euler's equation, which relates particle velocity to the pressure gradient. Active intensity is calculated using a combination of these two estimates. Configurations beyond a two-microphone probe have been explored, including multi-dimensional probes and the inclusion of center microphones.[12,13]

Two other energy-based acoustic quantities, reactive intensity and specific acoustic impedance, are also investigated in the current work. Reactive intensity is a vector pointing in the direction of the pressure gradient. It is a measure of the non-propagating energy per unit area in an acoustic field, where the pressure and particle velocity are in quadrature, exchanging potential and kinetic energy.[11] Reactive intensity is strong compared to active intensity in standing wave fields, in near fields, and in the presence of evanescent decay, and thus acts as a field indicator for these situations.[14] Specific acoustic impedance is a scalar quantity measuring the ratio of pressure to particle velocity for a given direction, often measured in ducts[15,16] but can also be applied to free fields.[17,18] It is used to estimate absorption and reflection properties of materials, and to characterize the radiation of structures. Similar to active intensity, both of these quantities rely on pressure and particle velocity estimates, and can be estimated for a single direction using a two-microphone probe.

In estimating energy-based quantities, each relies on a finite sum for center pressure estimation and a finite difference for center particle velocity estimation, which can result in estimation error. These errors occur for estimation in both the time and frequency domains. Finite-sum and finite-difference errors can occur at high frequencies as the wavelength becomes small compared to the microphone spacing, thus limiting high-frequency accuracy of the probe. These

errors were analyzed for active intensity in several fields by Thompson and Tree,[19] and a similar analysis was performed for specific acoustic impedance by Champoux and L'espérance.[20]

The accuracy bandwidth of energy-based quantity estimation is further limited by estimation error at low frequencies due to microphone phase mismatch,[10] This limitation requires that the microphone separation is carefully selected so the probe yields accurate estimates at the frequencies of interest and can even require the use of multiple probes with varying spacing if a broader frequency range is needed.

1.2 Prior Work

The phase and amplitude gradient estimator (PAGE) method was developed to reduce finite-sum and difference errors in active intensity estimation.[21] The details of the method are found in Sec. 2.2. By relying on the pressure amplitude and the phase gradient instead of the complex pressure, the accuracy bandwidth can be extended up to the spatial Nyquist frequency, the frequency at which the probe separation is equal to half a wavelength. Additionally, for broadband sources it is possible to unwrap the phase gradient, enabling accurate estimation beyond the spatial Nyquist frequency as long as there is sufficient coherence between the microphones. Phase unwrapping has been shown experimentally to allow an accuracy bandwidth of up to an order of magnitude greater than that of the traditional method.[22,23] The PAGE method has been applied to jet and rocket measurements,[24,25] loudspeaker measurements,[22] and to a real-time intensity-based localization system.[26] Additionally, performance of the method has been experimentally investigated for several two- and three-dimensional intensity probes.[27]

Whiting[28] presents initial research in understanding the analytical behavior of the PAGE method. In that work, he explores alternative probe configurations, including a three-microphone one-dimensional probe and several two-dimensional probes. In addition to active intensity, he

explores the performance of the PAGE method for other energy-based quantities, including reactive intensity and specific acoustic impedance. The performance is compared to the traditional method by deriving bias error expressions for two and three microphone probes. The current work expands on that analytical research, further exploring the performance of the PAGE method for two-microphone probes (Chapter 2), three-microphone probes (Chapter 3), and higher-order probes (Chapter 4), as well as providing experimental verification (Chapter 3) and extending the method for use in directional pressure sensing (Chapter 5).

In addition to the research presented here, current research explores several other aspects of the PAGE method. Work has been done to develop coherence-based unwrapping algorithms to prevent erroneous phase unwrapping for signals with low coherence.[29] Succo[30] explores the behavior of the PAGE method for narrowband signals, showing increased accuracy up to the spatial Nyquist frequency for harmonics of a sawtooth. Furthermore, the principles of the PAGE method have been applied to beamforming, extending bandwidth through phase unwrapping and array interpolation.[31]

1.3 Thesis Overview

This thesis presents research characterizing the PAGE method for use in energy-based quantity estimation and for direction finding. Chapter 2 provides a foundation for comparing the analytical performance of the PAGE and traditional methods by comparing bias errors in energy-based quantity estimation in several acoustic fields. This expands on the work done by Whiting by including expressions for a dipole field (Sec. 2.5) and introducing standardized notation and plots, and was published in the *Journal of the Acoustical Society of America* under the title "Bias error analysis for phase and amplitude gradient estimation of acoustic intensity and specific acoustic impedance."[32]

Chapter 3 explores the performance of a three-microphone probe, created by adding a center microphone. An experiment was performed to validate and compare the two and three-microphone bias errors. For each energy-based quantity a recommendation is given for the ideal microphone count and processing method. This research was published in the *Journal of the Acoustical Society of America* as an Express Letter under the title "Three-microphone probe bias errors for acoustic intensity and specific acoustic impedance."[33]

Chapter 4 investigates use of the PAGE method in reactive intensity estimation. Since the PAGE formulation of reactive intensity relies on the pressure gradient instead of the phase gradient, reactive intensity estimation accuracy is not aided by phase unwrapping. The use of additional microphones and higher-order derivatives to extend bandwidth is explored. Performance is analyzed for both a monopole field (Sec. 4.3) and a standing wave field (Sec. 4.4). This research was published in *Proceedings of Meetings on Acoustics* under the title "Higher-order estimation of active and reactive acoustic intensity."[34]

In Chapter 5, principles of the PAGE method are used to develop a phase gradient based method for directional pressure estimation. This allows for the creation of two-microphone directional pressure sensors with extended bandwidth and arbitrary array responses (Sec. 5.2). The performance of such a sensor is experimentally verified (Sec. 5.3). This research has been submitted to the *Journal of the Acoustical Society of America* as an Express Letter under the title "Highly directional pressure sensing using the phase gradient."

Chapter 6 summarizes the main conclusions from the research in this thesis, informing use of the PAGE method in various applications. Additionally, a summary of future work is given, including investigations of the effects of noise and the extension to other applications.

Chapter 2

Two-microphone bias errors

2.1 Introduction

Sound intensity is a vital measurement in energy-based acoustics, as can be seen from its use in sound power and source characterization and localization. Acoustic intensity cannot be measured directly, but is rather estimated using pressure and particle velocity. One method measures particle velocity directly using heated wires.[35] However, this sensor is sensitive to mean flow effects, which may make it less robust for outdoor measurements involving wind or temperature fluctuations (e.g., jet noise measurements).[36,37] Another method for estimating acoustic intensity uses microphone pairs and their cross spectra. In this formulation, pressure is estimated as the average measured pressure, and particle velocity is estimated using the pressure gradient across the microphones. This method, referred to in this article as the traditional method, was developed in the 1970s and is still in use today.[8-11] In an attempt to extend the frequency bandwidth of intensity calculations, the phase and amplitude gradient estimator method (PAGE) has been developed.[21] To provide an analytical foundation for the PAGE method, bias errors in calculations of active and reactive intensity and specific acoustic impedance using the PAGE method are compared to those of the traditional method. This chapter was modified from a 2017 paper published in the *Journal of the Acoustical Society of America* under the title "Bias error analysis for phase and amplitude gradient estimation of acoustic intensity and specific acoustic impedance."[32]

Several sources of error limit the bandwidth of intensity estimates using the traditional method. Low-frequency errors arise from phase and amplitude mismatch present in nonideal microphones,[10,38] whereas high-frequency errors arise from calculation bias errors inherent to the method caused by limitations in the finite-difference and finite-sum formulas,[11,19,39] as well as scattering from the microphones.[40-42] Of particular note to this paper is the work done by Fahy,[11] and Thompson and Tree,[19] who report bias errors from the traditional method of calculating active acoustic intensity for the fields created by several analytical sources.

A related quantity, specific acoustic impedance, can be used to determine the absorption of materials. As with intensity, the measurement depends on pressure and particle velocity, and can be estimated using two microphones in a similar manner. This method was developed first for use in tubes,[15,16] and later for free-field measurements.[17,18] An error analysis similar to that of Thompson and Tree has been carried out by Champoux and L'espérance[20] for free-field measurements of specific acoustic impedance.

Recently, the PAGE processing method has been shown experimentally to reduce, and in some cases completely remove, high-frequency calculation bias error from energy-based acoustic quantities.[28] Initial laboratory experimental validation of the method has been done,[22,23] and the method has been applied to jet and rocket noise measurements.[23-25] With the use of phase unwrapping, the PAGE method has extended the bandwidth of intensity measurements for broadband sources to be an order of magnitude greater than that of the traditional method.[23] In this work, we seek to validate the PAGE method analytically by examining its improvement of calculation bias errors over the traditional method.

Just as in the traditional method, the PAGE method estimates particle velocity by estimating the pressure gradient across multiple microphones. However, the amplitude and the

phase of the pressure are treated separately, resulting in a more robust method. In this paper, the two-microphone bias errors for the PAGE method are reported for three ideal fields: a plane wave, and fields from a monopole source and a dipole source. This investigation complements work of Fahy, Thompson and Tree, and Champoux and L'espérance by doing a similar analysis for the PAGE method, and extends their work by including reactive intensity. The PAGE method is shown to be more accurate at higher frequencies than the traditional method for active intensity and specific acoustic impedance, both with and without phase unwrapping.

2.2 Methodology

In order to show the advantages of using the PAGE processing method, the bias errors of the PAGE method for estimating intensity and specific acoustic impedance are reported and compared to those of the traditional method. An overview of the two methods is provided in this section.

Although more than two microphones can be used as shown by Cazzalato and Hansen[12] and Pascal and Li[13] for the traditional method, this paper considers only a two-microphone probe for one-dimensional quantity estimation. The frequency-dependent complex pressures at the locations of the two microphones are

$$p_1 = P_1 e^{j\phi_1}$$
$$p_2 = P_2 e^{j\phi_2} \tag{2.1}$$

with P denoting the magnitude and ϕ the phase at the location of the microphone. The microphones are in line with the source (as illustrated in Fig. 2.1), with microphone 1 closer to the source, and a distance d between the microphones. This paper considers only ideal point microphones, whereas in practice, high-frequency error would be introduced by scattering, which may include scattering from a solid spacer placed intentionally between the microphones.[40]

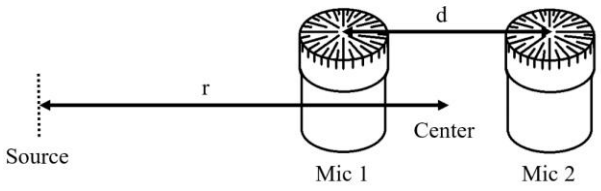

Figure 2.1. Schematic of a one-dimensional intensity probe consisting of two microphones. The probe axis points towards the source, such that the sound first passes microphone 1. The distance between the microphones is d.

Complex pressures obtained from microphone measurements are used to estimate acoustic quantities at the center of the probe, including pressure, acoustic particle velocity, active and reactive vector intensity and specific acoustic impedance. The center pressure is estimated as the average of the measured pressures. The acoustic particle velocity is found using Euler's equation,

$$\boldsymbol{u} = \frac{j}{\rho_0 \omega} \nabla p, \tag{2.2}$$

where ρ_0 is the density of air and ω the angular frequency. The bold font indicates a vector. The complex acoustic vector intensity is

$$\boldsymbol{I}_c = \frac{1}{2} p \boldsymbol{u}^*, \tag{2.3}$$

with * indicating complex conjugate. $\boldsymbol{I}_c$ can be separated into the active (real) and reactive (imaginary) parts,

$$\boldsymbol{I} = \frac{1}{2} \mathrm{Re}\{p \boldsymbol{u}^*\} \tag{2.4}$$

$$\boldsymbol{J} = \frac{1}{2} \mathrm{Im}\{p \boldsymbol{u}^*\}. \tag{2.5}$$

The factor of $1/2$ is due to the time or ensemble averaging of complex peak amplitudes [see Fahy[11] Eqs. (4.34c) and (4.34d)]. If using root-mean-square values instead of amplitudes, the factor of $1/2$ disappears. Finally, the complex specific acoustic impedance is

$$z = \frac{p}{u_e} \tag{2.6}$$

where u_e is the particle velocity in the direction the specific acoustic impedance is to be measured.

Once estimates of pressure and particle velocity are obtained, the intensity and impedance quantities in Eqs. (2.3)–(2.6) can be estimated. The following two subsections explain how these quantities are estimated for both the traditional and the PAGE processing methods.

2.2.1 Traditional method

The traditional method of measuring intensity and specific acoustic impedance has been in use for decades and is used in many measurement standards.[43,44] In this method, the complex pressure at the center of the probe, p, is estimated by averaging the real and imaginary parts of the complex pressures p_1 and p_2:

$$p^{\mathrm{TRAD}} = \frac{1}{2}(p_1 + p_2), \tag{2.7}$$

The traditional estimate of particle velocity is found from finite-differencing both the real and imaginary parts of the complex pressure:

$$\boldsymbol{u}^{\mathrm{TRAD}} = \frac{j}{\rho_0 \omega}\left(\frac{p_2 - p_1}{d}\right). \tag{2.8}$$

These estimated quantities, p^{TRAD} and $\boldsymbol{u}^{\mathrm{TRAD}}$ can exhibit bias errors when d becomes large relative to the acoustic wavelength. Bias errors associated with p^{TRAD} and $\boldsymbol{u}^{\mathrm{TRAD}}$ lead to bias errors in $\boldsymbol{I}^{\mathrm{TRAD}}$, $\boldsymbol{J}^{\mathrm{TRAD}}$ and z^{TRAD}. The traditional method bias errors are discussed in Sections 2.3 through 2.5 for the ideal planar, monopolar, and dipolar fields. These sections refer to the spatial Nyquist frequency, which is a limiting case where the microphone spacing equals half an acoustic wavelength. This occurs at $kd = \pi$ when the wave is incident along the probe axis.

2.2.2 PAGE method

To increase the reliable bandwidth of both pressure and particle velocity estimates, the PAGE method was developed.[21] The PAGE method estimates the complex pressure using phase and amplitude as,

$$p^{\mathrm{PAGE}} = \hat{P}e^{-j\hat{\phi}}, \tag{2.9}$$

where an overhat indicates an estimated quantity. Here, $\hat{P}$ is the estimated pressure amplitude at the center of the probe, computed as the mean of the pressure amplitudes of the two microphones,

$$\hat{P} = \frac{1}{2}(P_1 + P_2). \tag{2.10}$$

The center phase estimate $\hat{\phi}$ is a relative phase, and in practice it can be replaced with zero as it has no effect on energy-based quantities. Mann *et al.*[45] showed that when the complex pressure is expressed in terms of phase and amplitude, Euler's equation for particle velocity takes on a different form. Thomas *et al.*[21] used this formulation in the PAGE method to estimate particle velocity as

$$\boldsymbol{u}^{\mathrm{PAGE}} = \frac{e^{-j\hat{\phi}}}{\rho_0\omega}\left(\hat{P}\,\widehat{\nabla\phi} + j\widehat{\nabla P}\right), \tag{2.11}$$

The gradients of pressure amplitude and phase are estimated as

$$\widehat{\nabla P} = \frac{P_2 - P_1}{d} \tag{2.12}$$

$$\widehat{\nabla\phi} = \frac{\phi_2 - \phi_1}{d}. \tag{2.13}$$

When finding phase in practice, phase differences between the microphones are wrapped for $kd > \pi$, such that estimates of $\nabla\phi$ are incorrect. To find an accurate estimate of $\nabla\phi$, an unwrapping algorithm can be used on the phase difference as a function of frequency. Unwrapping can usually be successfully applied when the source is broadband with a smoothly varying phase and there is

sufficient coherence between the microphones.[23,31] The PAGE bias error equations reported in Sections 2.3 through 2.5 of this paper assume successful unwrapping. Without unwrapping, the bias errors would be different for $kd > \pi$.

The expressions for p^{PAGE} and $\boldsymbol{u}^{\mathrm{PAGE}}$ lead to expressions for $\boldsymbol{I}^{\mathrm{PAGE}}$, $\boldsymbol{J}^{\mathrm{PAGE}}$, and z^{PAGE}:

$$\boldsymbol{I}^{\mathrm{PAGE}} = \frac{\hat{P}^2 \widehat{\nabla\phi}}{2\rho_0 \omega} \tag{2.14}$$

$$\boldsymbol{J}^{\mathrm{PAGE}} = -\frac{\hat{P}\, \widehat{\nabla P}}{2\rho_0 \omega} \tag{2.15}$$

$$z^{\mathrm{PAGE}} = \frac{\hat{P}\rho_0 \omega}{\left[\hat{P}\widehat{\nabla\phi} + j\widehat{\nabla P}\right] \cdot \hat{\boldsymbol{e}}} = \frac{\hat{P}^2}{2\boldsymbol{I}_c^* \cdot \hat{\boldsymbol{e}}} \tag{2.16}$$

The expression for active intensity in Eq. (2.14) has been reported previously by Mechel,[46] although with the development of the PAGE method, this formulation has progressed to a measurement tool. The estimate of specific acoustic impedance in Eq. (2.16) is in a particular direction, denoted by the unit vector $\hat{\boldsymbol{e}}$. The remainder of this paper compares performance of the traditional and PAGE methods for a plane wave, a monopole source, and a dipole source. This systematic evaluation of the bias errors for these propagating wave fields provides an analytical foundation for the PAGE method that can guide future application and development.

2.3 Plane wave

This section reports bias errors for a plane wave. A plane wave is an ideal field with p and u in phase, similar to the far-field behavior of many acoustic sources. Errors in traditional and PAGE estimates of p and $\boldsymbol{u}$ lead to errors in $\boldsymbol{I}$ and z, all of which are reported. Since a plane wave has zero reactive intensity, $\boldsymbol{J}$ is not discussed in this section.

2.3.1 Pressure

The complex pressure of a plane wave can be represented as $p = Ae^{-jkx}$, where A is the amplitude, x is the distance from the origin, and $k = \omega/c$ is the acoustic wavenumber. The traditional method estimates the pressure at the center of the intensity probe by averaging the real and imaginary parts of the frequency-dependent complex pressure, which vary in space. Fahy[11] evaluates the traditional method bias error by considering the error ratio of estimated pressure over actual pressure [see his Eq. (5.40a)]:

$$\frac{p^{\mathrm{TRAD}}}{p} = \cos(kd/2). \tag{2.17}$$

The traditional method bias error level, $L_{\varepsilon,p} = 20\log_{10}\left(\left|p^{\mathrm{TRAD}}/p\right|\right)$, is plotted as a function of kd in Fig. 2.2(a). The phase of the error ratio is shown in Fig. 2.2(b). The error is nearly zero for small values of kd, but the error increases as kd approaches the spatial Nyquist limit of π. Previous authors have given differing criteria for acceptable error, although in this work we will use Fahy's criterion of less than 5% error.[11] The error in pressure is less than 5% (about 0.4 dB) for $kd < 0.64$.

In contrast, the PAGE formulation given in Eq. (2.9) estimates the correct pressure amplitude at all frequencies, which is also shown in Fig. 2.2(a). As shown in Fig. 2.2(b), the phase is correct above $kd = \pi$ only if unwrapping is applied, but since only pressure magnitude is used for $\boldsymbol{I}^{\mathrm{PAGE}}$ and z^{PAGE}, phase error has no effect on these estimates.

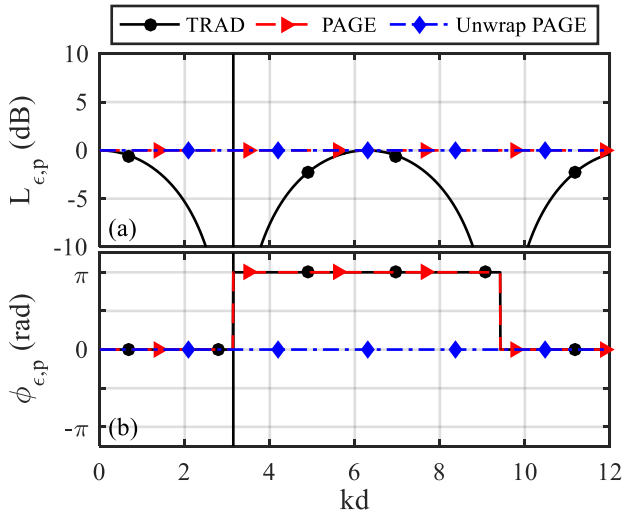

Figure 2.2. Bias errors in estimates of center pressure (a) amplitude and (b) phase of a plane wave as a function of kd using the traditional method, p^{TRAD}, and the PAGE method, p^{PAGE}, without and with phase unwrapping. The solid, vertical line is the spatial Nyquist frequency.

2.3.2 Particle velocity

For the plane wave case, the analytical particle velocity differs from the pressure by a factor of $\rho_0 c$,

$$\boldsymbol{u} = \frac{A}{\rho_0 c} e^{-jkx}\, \hat{\boldsymbol{x}}, \tag{2.18}$$

where $\hat{\boldsymbol{x}}$ is the unit vector in the direction of propagation. Fahy[11] [Eq. (5.40b)] gives the traditional method error ratio as

$$\frac{\boldsymbol{u}^{\mathrm{TRAD}}}{\boldsymbol{u}} = \mathrm{sinc}(kd/2). \tag{2.19}$$

The error (one minus the error ratio) is low for small kd and grows more slowly than the pressure error given in Eq. (2.17). The error level, $L_{\varepsilon,u} = 20\log_{10}\left(\left|\boldsymbol{u}^{\mathrm{TRAD}}/\boldsymbol{u}\right|\right)$, is plotted in Fig. 2.3(a) and is less than 5% (0.4 dB) for $kd < 1.1$.

The PAGE method estimate of particle velocity given in Eq. (2.11) has zero error up to $kd = \pi$. Without phase unwrapping, errors in the estimate of $\nabla\phi$ lead to bias errors in amplitude

for $kd > \pi$ and phase for $kd > 2\pi$. For cases where phase unwrapping may be applied, however, $\boldsymbol{u}^{\mathrm{PAGE}}$ has zero error for $kd > \pi$.

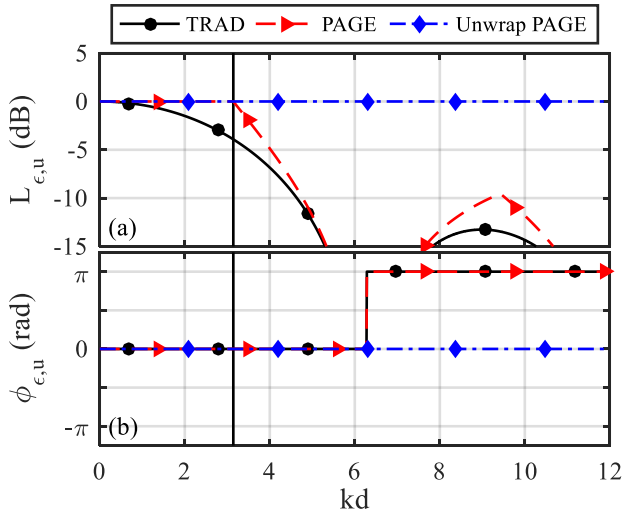

Figure 2.3. Bias errors in estimates of particle velocity (a) amplitude and (b) phase of a plane wave as a function of kd using the traditional method, $\boldsymbol{u}^{TRAD}$, and the PAGE method, $\boldsymbol{u}^{PAGE}$, without and with phase unwrapping. The solid, vertical line is the spatial Nyquist frequency.

2.3.3 Active intensity

Bias errors in both the estimates of p and $\boldsymbol{u}$ contribute to bias errors in $\boldsymbol{I}$. Analytically, the active intensity of a plane wave of amplitude A is $\boldsymbol{I} = A^2/2\rho_0 c$. By combining the bias errors in Eqs. (2.17) and (2.19) and simplifying, the traditional method bias error for active intensity is found to be

$$\frac{\boldsymbol{I}^{\mathrm{TRAD}}}{\boldsymbol{I}} = \mathrm{sinc}(kd). \tag{2.20}$$

Figure 2.4 shows the error level $L_{\varepsilon,I} = 10\log_{10}\left(\left|\boldsymbol{I}^{\mathrm{TRAD}}/\boldsymbol{I}\right|\right)$ as well as the phase error. For the traditional method, the error in active intensity is less than 5% (0.2 dB) for $kd < 0.55$—half the range for particle velocity. The direction of $\boldsymbol{I}^{\mathrm{TRAD}}$ is correct until $kd = \pi$. $\boldsymbol{I}^{\mathrm{PAGE}}$ has zero error up to $kd = \pi$ because there was zero error in p and $\boldsymbol{u}$. If the phase is unwrapped, there is zero error for any kd.

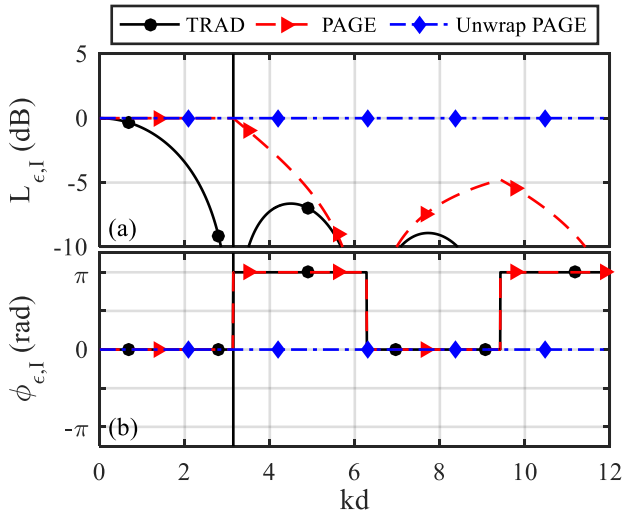

Figure 2.4. Bias errors in estimates of active intensity (a) magnitude and (b) direction of a plane wave as a function of kd using the traditional method, $\boldsymbol{I}^{TRAD}$, and the PAGE method, $\boldsymbol{I}^{PAGE}$, without and with phase unwrapping.

2.3.4 Specific acoustic impedance

The specific acoustic impedance of a plane wave is $z = \rho_0 c$. The bias errors in z depend on the bias errors in estimates of p and $\boldsymbol{u}$, and result in an expression equivalent to one given by Champoux and L'espérance[20] [see Eq. (12) in that paper]:

$$\frac{\mathrm{z}^{\mathrm{TRAD}}}{z} = \frac{\cos(kd/2)}{\mathrm{sinc}(kd/2)}. \tag{2.21}$$

The error level $L_{\varepsilon,z} = 20\log_{10}\left(\left|z^{\mathrm{TRAD}}/z\right|\right)$ and the phase error are shown in Fig. 2.5. For the traditional method, the error in specific acoustic impedance is less than 5% (0.4 dB) for $kd < 0.77$, whereas the phase remains correct until spatial aliasing occurs at $kd = \pi$. Since the PAGE method with phase unwrapping has no errors in pressure or particle velocity, there are no errors in z^{PAGE}, even above $kd = \pi$.

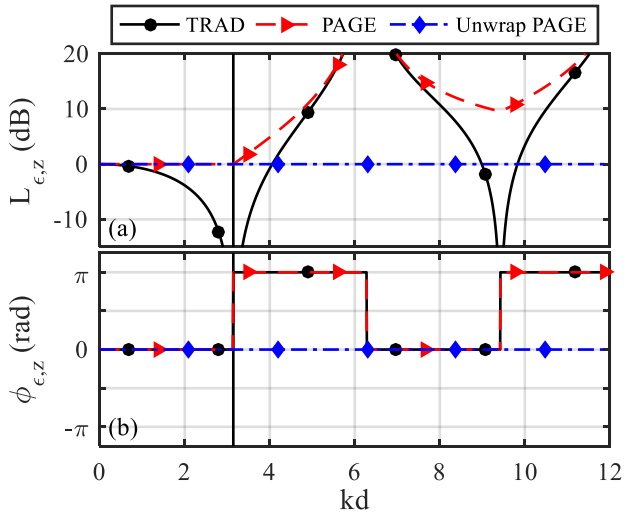

Figure 2.5. Bias errors in estimates of specific acoustic impedance (a) amplitude and (b) phase of a plane wave as a function of kd using the traditional method, z^{TRAD}, and the PAGE method, z^{PAGE}, without and with phase unwrapping.

In summary for the plane wave case, traditional estimates of acoustic quantities have increasing error as kd increases. Table 2.1 shows the maximum value of kd that has less than 5% error for traditional estimation of each quantity. The approximate bandwidth for active intensity is limited to $kd < 0.55$, and for specific acoustic impedance to $kd < 0.77$, both of which are well below the spatial Nyquist frequency of $kd = \pi$. In contrast, the PAGE estimates are accurate up to $kd = \pi$, and if unwrapping is successfully applied, there are no bias errors at any kd. The absence of bias errors for the planar case is significant because many propagating sound fields can be approximated as planar at distances sufficiently far from the source. This was verified experimentally in previous work[23] where the bandwidth of active intensity calculations using the PAGE method was extended at least an order of magnitude past the traditional method. For very high frequencies, the method broke down due to insufficient coherence between the microphones.

Table 2.1. The maximum value of kd for each quantity that results in less than 5% error in a plane-wave field using traditional processing. PAGE processing has no error up to $kd = \pi$ for each quantity, and is accurate beyond that if unwrapping is successfully applied.

Quantity	TRAD kd limit
p	0.64
$\boldsymbol{u}$	1.1
$\boldsymbol{I}$	0.55
z	0.77

2.4 Monopole source

Examining the traditional and PAGE bias errors in a monopole-radiated field shows how these methods perform in both near and far-field environments. Unlike the plane-wave case, where there is no near field, the bias errors for the monopole case depend on both the size of the probe, d, and the distance from the source, r.

2.4.1 Pressure

The analytical expression for the complex pressure a distance r from a monopole with amplitude A is $p = Ae^{-jkr}/r$. The traditional method error ratio for center pressure, based on Eq. (2.7), is

$$\frac{p^{\mathrm{TRAD}}}{p} = \frac{1}{1-\beta^2/4}\left[\cos(kd/2) + \frac{j\beta}{2}\sin(kd/2)\right], \tag{2.22}$$

where

$$\beta = \frac{kd}{kr}. \tag{2.23}$$

The PAGE method formulation given in Eq. (2.9) results in an estimated-to-analytical ratio for the monopole field of

$$\frac{p^{\mathrm{PAGE}}}{p} = \frac{1}{1-\beta^2/4}. \tag{2.24}$$

Unlike the plane-wave case, the bias error in p^{PAGE} is nonzero and depends on the ratio β for the monopole source. A large value of β means the probe is close to the source relative to the microphone spacing, with a limit of $\beta = 2$. The value of β approaches zero as the microphone spacing becomes small or the distance from the source becomes large.

The monopole pressure bias errors in Eqs. (2.22) and (2.24) are equivalent to the plane wave pressure bias errors shown in Fig. 2.2 for the far-field case of $\beta = 0$. For nonzero values of β, error is introduced even at low values of kd. Both methods have greater than 5% error when $\beta > 0.44$, although the traditional method has additional error for large kd, as in the monopole case. If unwrapping is applied to broadband signals, the PAGE method has the correct phase past $kd = \pi$.

2.4.2 Particle velocity

The analytical expression of the acoustic particle velocity a distance r from a monopole source is

$$\boldsymbol{u} = \frac{A(-j+kr)}{\rho_0 \omega}\frac{e^{-jkr}}{r^2}\hat{\boldsymbol{r}}, \tag{2.25}$$

where $\hat{\boldsymbol{r}}$ is the unit vector pointing away from the source. The ratio of the traditional estimate of the acoustic particle velocity [calculated using Eq. (2.8)] to the analytical expression is

$$\frac{\boldsymbol{u}^{\mathrm{TRAD}}}{\boldsymbol{u}} = \frac{1}{1-\beta^2/4}\frac{jkr\,\mathrm{sinc}(kd/2)+\cos(kd/2)}{(1+jkr)}. \tag{2.26}$$

From Eq. (2.11), the PAGE method error ratio is

$$\frac{\boldsymbol{u}^{\mathrm{PAGE}}}{\boldsymbol{u}} = \frac{1}{1-\beta^2/4}. \tag{2.27}$$

Similar to the bias errors in the center pressure, estimates in the monopole field, $\boldsymbol{u}^{\mathrm{TRAD}}$ and $\boldsymbol{u}^{\mathrm{PAGE}}$, have nonzero bias errors for small kd, which depend on β. The PAGE method maintains constant bias error up to $kd = \pi$ equal to the pressure bias error, and is constant for all frequencies if unwrapping is applied.

2.4.3 Active intensity

From the expressions for pressure and particle velocity, the analytical expression for active intensity radiated from a monopole source with amplitude A is

$$\boldsymbol{I} = \frac{A^2}{2\rho_0 c r^2}\,\hat{\boldsymbol{r}}. \tag{2.28}$$

The traditional method's intensity error ratio for a monopole is similar to the plane wave [see Eq. (2.20)] but with an additional factor that depends on β. The ratio is reported by Thompson and Tree[19] [see their Eq. (14)] to be

$$\frac{\boldsymbol{I}^{\mathrm{TRAD}}}{\boldsymbol{I}} = \frac{1}{1-\beta^2/4}\mathrm{sinc}(kd). \tag{2.29}$$

The PAGE method error ratio calculated using Eq. (2.14) is

$$\frac{\boldsymbol{I}^{\mathrm{PAGE}}}{\boldsymbol{I}} = \left(\frac{1}{1-\beta^2/4}\right)^2, \tag{2.30}$$

which is frequency independent but does depend on β. This bias error in Eq. (2.30) is larger than the bias error of the traditional method in Eq. (2.29) at low values of kd.

Since the active intensity of the sound field from a monopole source depends on both the size of the probe, d, and the distance from the source, r, it is useful to plot the bias errors as a function of both variables. The kd versus kr plots in Fig. 2.6 show the bias errors in (a) $\boldsymbol{I}^{\mathrm{TRAD}}$and (b) $\boldsymbol{I}^{\mathrm{PAGE}}$ with phase unwrapping. Lines of constant β run diagonally, over which only the frequency varies.

Both methods have significant errors close to the source as kr approaches $kd/2$ and β approaches 2. Far from the source, both methods approach zero error as β approaches 0. Both plots in Fig. 2.6 have a solid, black line tracing the limit of 5% error. At low kd, the traditional method has less than 5% error when $\beta < 0.44$. The bias errors in $\boldsymbol{I}^{\mathrm{TRAD}}$ are large as kd increases, and when kr is also large, the results converge to the plane wave case with less than 5% error for $kd < 0.55$. The PAGE method maintains constant error over frequency, with less than 5% error when $\beta < 0.31$. If a 50 mm microphone spacing is used, this corresponds to a minimum distance from the center of the probe to the source of 160 mm. At low frequencies, the traditional method outperforms the PAGE method, although the difference is negligible except over a small range of near-field locations corresponding to $0.31 < \beta < 0.44$ where the traditional method is within 5% error and the PAGE method is not. Otherwise, the PAGE method, with its extended bandwidth is preferable.

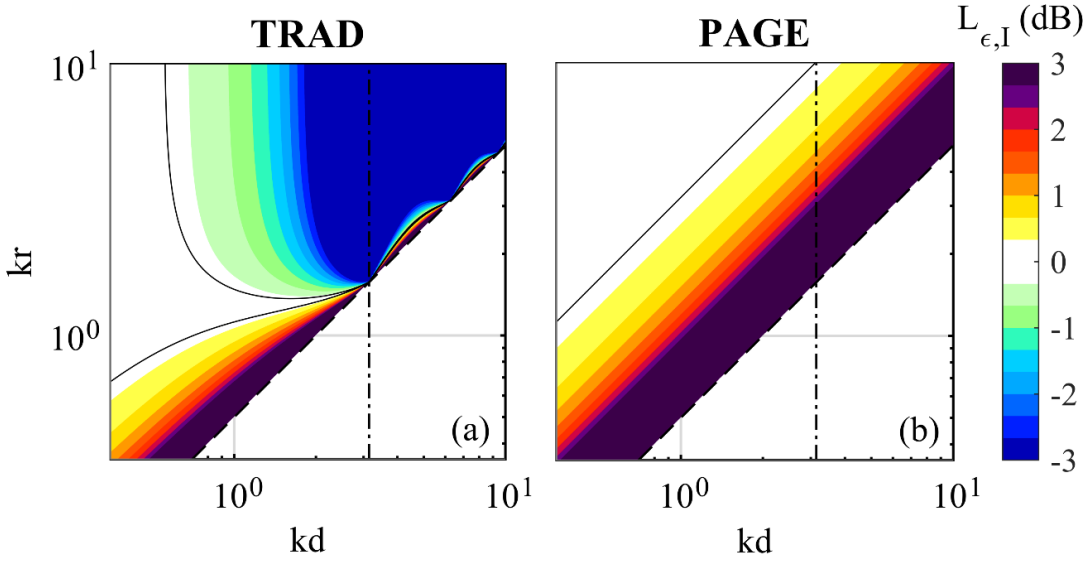

Figure 2.6. Bias errors in estimates of the magnitude of active intensity for a monopole field as a function of kd *and* kr*: (a)* $\boldsymbol{I}^{TRAD}$ *and (b) unwrapped* $\boldsymbol{I}^{PAGE}$*. The vertical dashed line is the spatial Nyquist limit. To the left of this line, wrapped and unwrapped PAGE give the same results. The diagonal dashed line follows* $r = \mathrm{d}/2$*. The solid black lines trace the limit of* 5% *error.*

2.4.4 Reactive intensity

The bias errors for the reactive intensity of the sound field from a monopole source also depend on β. The analytical expression for reactive intensity from a monopole source is

$$\boldsymbol{J} = \frac{A^2}{2\rho_0 \omega r^3}\hat{\boldsymbol{r}}. \tag{2.31}$$

For a two-microphone probe, expressions for $\boldsymbol{J}^{\mathrm{TRAD}}$ and $\boldsymbol{J}^{\mathrm{PAGE}}$ are equivalent regardless of the field, since both methods result in an expression involving a difference in autospectra.[28] However, since reactive intensity bias errors have not been previously reported in the literature, it is worthwhile to report them here. The reactive intensity error ratios are

$$\frac{\boldsymbol{J}^{\mathrm{TRAD}}}{\boldsymbol{J}} = \frac{\boldsymbol{J}^{\mathrm{PAGE}}}{\boldsymbol{J}} = \left(\frac{1}{1-\beta^2/4}\right)^2, \tag{2.32}$$

The reactive intensity bias errors for both methods are plotted in Fig. 2.7. Both estimates, (a) $\boldsymbol{J}^{\mathrm{TRAD}}$ and (b) $\boldsymbol{J}^{\mathrm{PAGE}}$ have less than 5% error for $\beta < 0.31$, and infinite error as r approaches $d/2$.

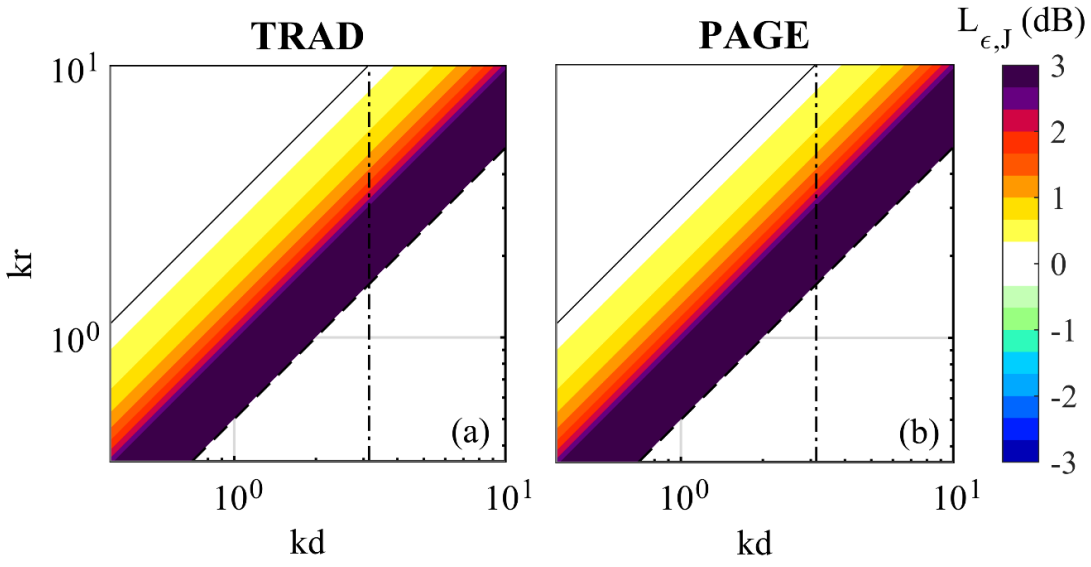

Figure 2.7. Bias errors in estimates of the magnitude of reactive intensity for a monopole field as a function of kd and kr: (a) $\boldsymbol{J}^{TRAD}$ and (b) $\boldsymbol{J}^{PAGE}$. The vertical dashed line is the spatial Nyquist limit. The diagonal dashed line follows $r = d/2$. The solid black line traces the limit of 5% error.

2.4.5 Specific acoustic impedance

The analytical expression for the specific acoustic impedance in the radial direction for a monopole field is

$$z = \frac{\rho_0 ckr}{kr - j} \tag{2.33}$$

The error ratio for z^{TRAD} can be found from the ratios for p^{TRAD} and $\boldsymbol{u}^{\mathrm{TRAD}}$, given in Eqs. (2.22) and (2.26), respectively. The resulting expression matches (with some reworking and allowance for a typographical error) an expression given by Champoux and L'espérance[20] [see their Eq. (11)]:

$$\frac{z^{\mathrm{TRAD}}}{z} = \beta \frac{(1 + jkr)[2\cos(kd/2) + j\beta \sin(kd/2)]}{2[\beta \cos(kd/2) + j2 \sin(kd/2)]}. \tag{2.34}$$

For the PAGE processing method, the bias errors in p^{PAGE} [Eq. (2.24)] and $\boldsymbol{u}^{\mathrm{PAGE}}$ [Eq. (2.27)] are identical, which cancel out in the estimation of z^{PAGE}. This means that regardless of distance from the source, there is zero error in specific acoustic impedance or in any impedance-based quantities such as absorption. This is true up to $kd = \pi$, and for all frequencies where unwrapping is successfully applied. Figure 2.8(a) shows the bias errors for the traditional method as a function of kd and kr. The traditional estimate z^{TRAD} has large errors at high frequencies (near and above $kd = \pi$), whereas z^{PAGE} has no bias errors, shown in Fig. 2.8(b).

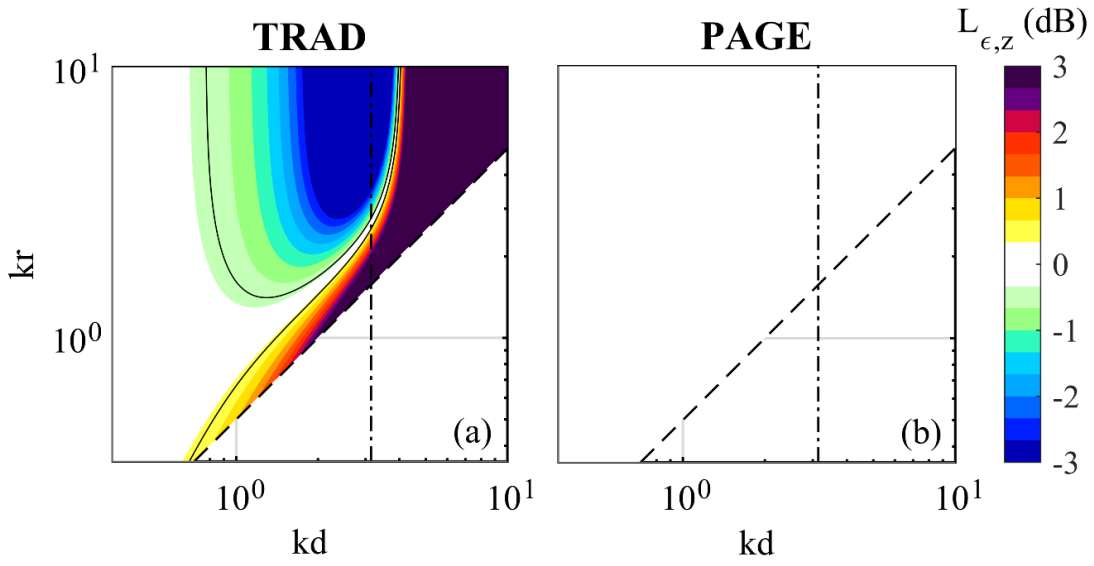

Figure 2.8. Bias errors in estimates of the amplitude of specific acoustic impedance for a monopole field as a function of kd *and* kr*: (a)* z^{TRAD}*, and (b) unwrapped* z^{PAGE}*. The vertical dashed line is the spatial Nyquist limit. To the left of this line, wrapped and unwrapped PAGE give the same results. The diagonal dashed line follows* $r = d/2$*. The solid black lines trace the limit of* 5% *error.*

To summarize the bias errors for the monopole case, the errors depend not only on kd as seen in the plane wave case, but also on the ratio β. In the case of active intensity, the PAGE method is somewhat more limited in terms of how close the probe can be to the source. However, for all the quantities reported except reactive intensity, the traditional method has increasing errors as kd approaches π, whereas the PAGE method error does not change as kd approaches π for any quantity. With unwrapping, the PAGE error in active intensity remains constant as a function of β for frequencies past $kd = \pi$, and the specific acoustic impedance estimate has zero bias error.

2.5 Dipole source

The final case considered is the field from an acoustic dipole, defined to be two out-of-phase sources with equal amplitudes and closely spaced such that their spacing is much smaller than a wavelength. A dipole creates a highly reactive near field, with a pressure term that decays as $1/r^2$, in addition to the $1/r$ term that is present for the monopole. Furthermore, the particle velocity has terms that decay as $1/r^3$, $1/r^2$, and $1/r$. Thus, there is a stronger distinction between

the near and far fields and greater opportunities to observe bias errors in the intensity and specific acoustic impedance estimates.

2.5.1 Pressure

In addition to dependence on radial distance r, the dipole field varies with the angle θ from the dipole axis. The analytical expression for the complex pressure at location (r, θ) is written as[11]

$$p = A\cos(\theta)\frac{1+jkr}{r^2}e^{-jkr}, \tag{2.35}$$

where A is the dipole moment source strength. Assuming the two-microphone probe axis is pointed at the center of the dipole, the angular dependence of p in Eq. (2.35) can be separated from the radial dependence, and the bias errors are independent of θ.

For the two-microphone probe the ratio of traditionally estimated pressure [Eq. (2.7)] to Eq. (2.35) is

$$\frac{p^{\mathrm{TRAD}}}{p} = \frac{[1+jkr+(1-jkr)\beta^2/4]\cos(kd/2)+[j\beta-kd(1-\beta^2/4)/2]\sin(kd/2)}{(1-\beta^2/4)^2(1+jkr)}. \tag{2.36}$$

For the PAGE formulation [Eq. (2.9)], the estimated-to-analytical ratio is

$$\frac{p^{\mathrm{PAGE}}}{p} = \frac{(kr)^2(P_1+P_2)}{2(1+jkr)}e^{j(\alpha_1+\alpha_2)/2}, \tag{2.37}$$

where

$$\begin{aligned} P_1 &= \frac{\sqrt{1+(kr-kd/2)^2}}{(kr-kd/2)^2} \\ P_2 &= \frac{\sqrt{1+(kr+kd/2)^2}}{(kr+kd/2)^2}, \end{aligned} \tag{2.38}$$

which are the pressure amplitudes at microphone locations 1 and 2 for the dipole case [with the amplitude terms A and $\cos(\theta)$ omitted]. Additionally,

$$\alpha_1 = \arctan(kr - kd/2)$$
$$\alpha_2 = \arctan(kr + kd/2). \tag{2.39}$$

For large values of kr, the probe is in the far field where the pressure amplitude has a $1/r$ dependence rather than a $1/r^2$ dependence. In this case, the dipole pressure bias errors in Eqs. (2.36) and (2.37) converge to Eqs. (2.22) and (2.24) for the monopole case. Otherwise, the dipole bias errors are larger than the monopole bias errors for both methods, dependent on kr. Bias errors in p^{TRAD} oscillate similar to the plane wave and the monopole cases, severely limiting the usable bandwidth. Bias errors in p^{PAGE} also change, but the error decreases as frequency increases.

2.5.2 Particle velocity

The radial component of the particle velocity is

$$\boldsymbol{u}_r = A\cos(\theta)\frac{-2j + kr(2 + jkr)}{ckr^3\rho_0}e^{-jkr}\hat{\boldsymbol{r}} \tag{2.40}$$

With the probe oriented towards the center of the dipole, only the radial component of particle velocity is estimated. The angular dependence cancels out in the traditional estimated-to-analytical ratio. Using Eq. (2.8), this ratio is

$$\frac{\boldsymbol{u}_r^{\mathrm{TRAD}}}{\boldsymbol{u}_r} = \frac{[j\beta - kd(1 - \beta^2/4)/2]\cos(kd/2) - [1 + jkr + (1 - jkr)\beta^2/4]\sin(kd/2)}{(1 - \beta^2/4)^2[-2j + kr(2 + jkr)]\beta/2}. \tag{2.41}$$

The PAGE estimated-to-analytical ratio for the particle velocity, based on Eq. (2.11), is

$$\frac{\boldsymbol{u}_r^{\mathrm{PAGE}}}{\boldsymbol{u}_r} = \frac{(kr)^2[2j(P_2 - P_1) + (P_1 + P_2)(kd + \alpha_1 - \alpha_2)]}{[-2j + kr(2 + jkr)]2\beta}e^{j(\alpha_1 + \alpha_2)/2}. \tag{2.42}$$

As with pressure, the dipole case shows increased error for low kr and a convergence to the monopole case for high kr.

2.5.3 Active intensity

The radial component of the active intensity for the dipole is obtained from the expression for pressure in Eq. (2.35) and for particle velocity in Eq. (2.40). The active intensity may be written as

$$\boldsymbol{I}_r = \frac{k^2 A^2 \cos^2\theta}{2cr^2\rho_0}\hat{\mathbf{r}}. \tag{2.43}$$

Again, the angular dependence is independent of the $1/r^2$ radial dependence, such that a one-dimensional probe can obtain the radially dependent active intensity.

The traditional method has an estimated-to-analytical intensity ratio of

$$\frac{\boldsymbol{I}_r^{\mathrm{TRAD}}}{\boldsymbol{I}_r} = \frac{kd\cos(kd) - [1 + (kr)^2(1 - \beta^2/4)]\sin(kd)}{kd(kr)^2(1 - \beta^2/4)^2}, \tag{2.44}$$

which is equivalent to an expression given by Thompson and Tree[19] [see their Eq. (18)]. The PAGE processing method, calculated using Eq. (2.14), has a ratio of

$$\frac{\boldsymbol{I}_r^{\mathrm{PAGE}}}{\boldsymbol{I}_r} = -\frac{kr}{4\beta}(P_1 + P_2)^2(-kd + \alpha_2 - \alpha_1). \tag{2.45}$$

The bias errors in the magnitude of $\boldsymbol{I}_r$ depend on both kd and kr, as displayed in Fig. 2.9. As r approaches d (below $kd = \pi$), the bias error in $\boldsymbol{I}_r^{\mathrm{PAGE}}$increases more rapidly than for $\boldsymbol{I}_r^{\mathrm{TRAD}}$, similar to the monopole case. As kd increases, $\boldsymbol{I}_r^{\mathrm{TRAD}}$ underestimates the magnitude of $\boldsymbol{I}_r$. Using PAGE processing, $\boldsymbol{I}_r^{\mathrm{PAGE}}$ (with phase unwrapping) has less than 5% error at low kr if $\beta < 0.18$, and for high kr the limit is the same as the monopole case, namely $\beta < 0.31$.

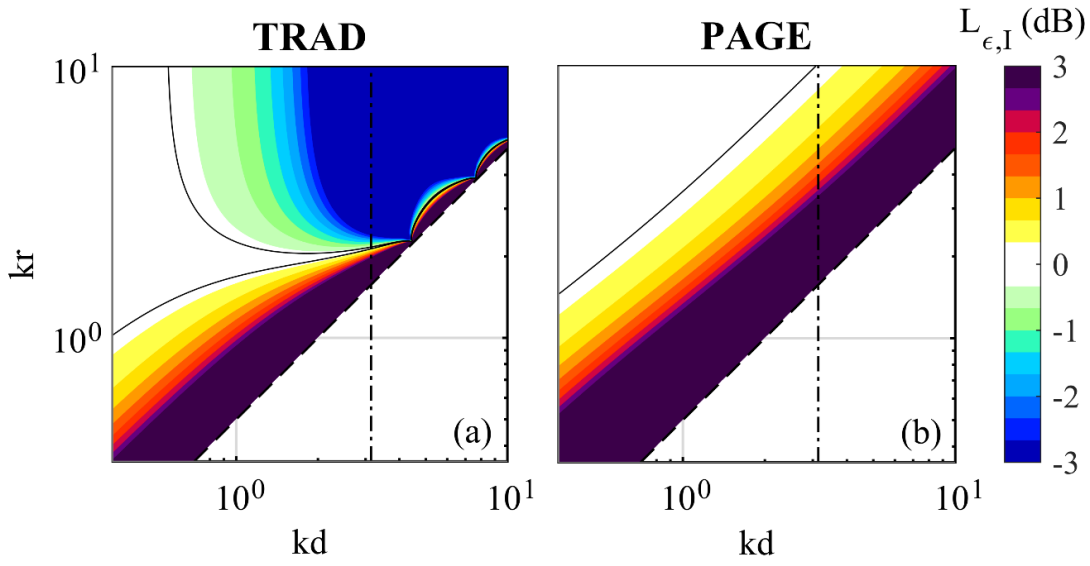

Figure 2.9. Bias errors in estimates of the magnitude of active intensity for a dipole field as a function of kd *and* kr*: (a)* $\boldsymbol{I}^{TRAD}$*, and (b) unwrapped* $\boldsymbol{I}^{PAGE}$*. The vertical dashed line is the spatial Nyquist limit. To the left of this line, wrapped and unwrapped PAGE give the same results. The diagonal dashed line follows* $r = d/2$*. The solid black lines trace the limit of* 5% *error.*

2.5.4 Reactive intensity

The analytical expression for the radial component of the reactive intensity is

$$\boldsymbol{J}_r = \frac{2 + (kr)^2}{2\omega r^5 \rho_0} A^2 \cos^2\theta\, \hat{\boldsymbol{r}}. \tag{2.46}$$

The traditional and PAGE processing methods produce the same estimated-to-analytical ratio:

$$\frac{\boldsymbol{J}_r^{\text{TRAD}}}{\boldsymbol{J}_r} = \frac{\boldsymbol{J}_r^{\text{PAGE}}}{\boldsymbol{J}_r} = \frac{1}{(1-\beta^2/4)^4}\left[1 + \frac{\beta^2[1 + (kd)^2/8 - (kr)^2]}{2[2 + (kr)^2]}\right]. \tag{2.47}$$

Figure 2.10 shows this bias error as a function of kd and kr. There is less than 5% error for low kr if $\beta < 0.20$, and for high kr it converges to the monopole case of $\beta < 0.31$.

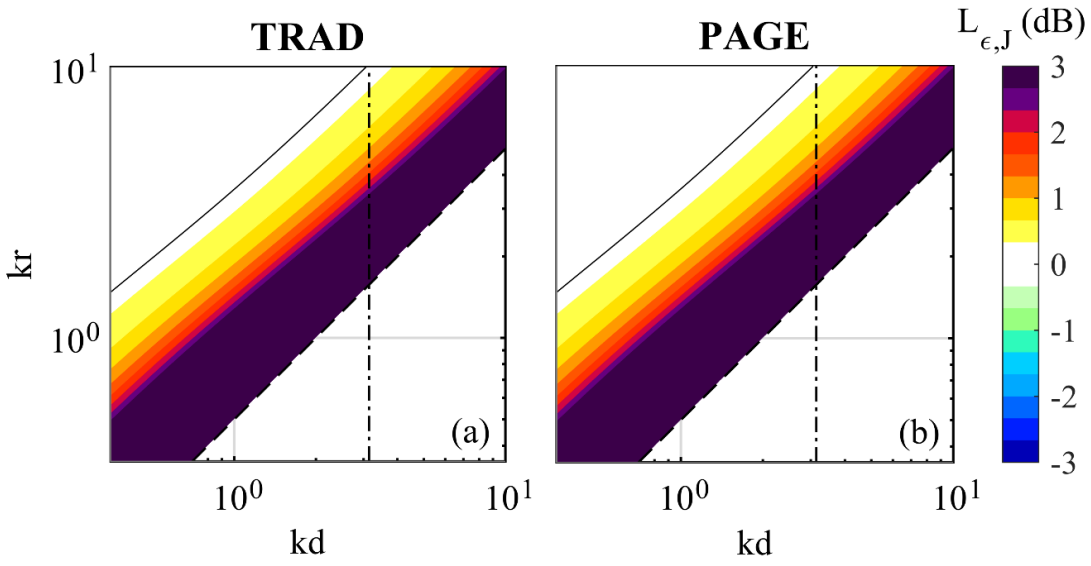

Figure 2.10. Bias errors in estimates of the magnitude of reactive intensity for a dipole field as a function of kd *and* kr*: (a)* $\boldsymbol{J}^{TRAD}$ *and (b)* $\boldsymbol{J}^{PAGE}$*. The vertical dashed line is the spatial Nyquist limit. The diagonal dashed line follows* $r = d/2$*. The solid black line traces the limit of* 5% *error.*

2.5.5 Specific acoustic impedance

The last quantity to consider is the specific acoustic impedance. The analytical expression for the dipole case is

$$z = \frac{\omega\rho_0 r(1+jkr)}{-2j+kr(2+jkr)}. \tag{2.48}$$

The estimated-to-analytical ratio for the traditional method is

$$\frac{z^{\mathrm{TRAD}}}{z} = \frac{[-2j+kr(2+jkr)]\beta}{2(1+jkr)}\left[\frac{[1+jkr+(1-jkr)\beta^2/4]\cos(kd/2)+[j\beta-kd(1-\beta^2/4)/2]\sin(kd/2)}{[j\beta-kd(1-\beta^2/4)/2]\cos(kd/2)-[1+jkr+(1-jkr)\beta^2/4]\sin(kd/2)}\right]. \tag{2.49}$$

Although the PAGE method had zero error for the plane wave and monopole cases, bias errors in p^{PAGE} [Eq. (2.37)] and $\boldsymbol{u}^{\mathrm{PAGE}}$ [Eq. (2.42)] are not identical for the dipole case. Combining the errors results in the ratio

$$\frac{z^{\mathrm{PAGE}}}{z} = \frac{\beta[-2j + kr(2 + jkr)](P_1 + P_2)}{(1 + jkr)[2j(P_2 - P_1) + (P_1 + P_2)(kd + \alpha_1 - \alpha_2)]}. \tag{2.50}$$

Figure 2.11 shows the bias errors for specific acoustic impedance. Approaching $kd = \pi$, the traditional method has increasingly large errors. In contrast, the PAGE method has decreasing error above $kd = \pi$, and has less than 5% error for all values of kd if $\beta < 0.45$.

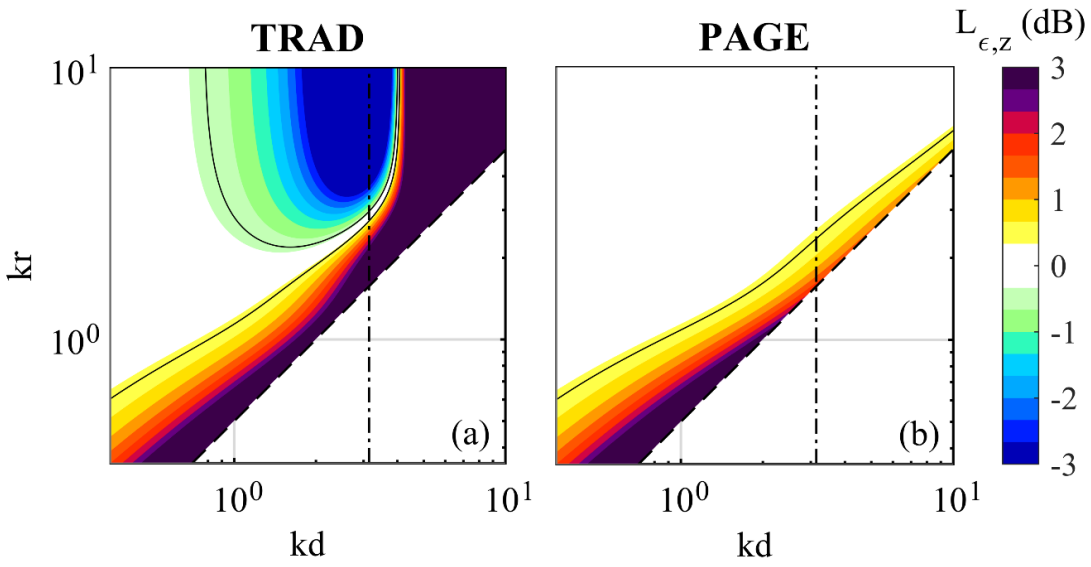

Figure 2.11. Bias errors in estimates of the amplitude of specific acoustic impedance for a dipole field as a function of kd and kr: (a) z^{TRAD}, and (b) unwrapped z^{PAGE}. The vertical dashed line is the spatial Nyquist limit. To the left of this line, wrapped and unwrapped PAGE give the same results. The diagonal dashed line follows $r = d/2$. The solid black lines trace the limit of 5% error.

In summary, this bias error analysis for the case of the acoustic dipole provides insights into the near-field performance of the traditional and PAGE estimates of intensity and impedance. For active intensity, there is a small range of β values over which traditional estimates at low frequencies have less than 5% error and the PAGE estimates do not. However, not only is PAGE comparable outside this narrow range but it also has the advantage of decreasing error with increasing frequency, as opposed to the traditional method, which has increasing error with increasing frequency and becomes unusable much before $kd = \pi$. The extended bandwidth of the PAGE estimates are advantageous when calculating the intensity and specific acoustic impedance

from an acoustic dipole, and when unwrapping can be applied, this advantage is even more pronounced.

2.6 Conclusion

Analytical bias error calculations for simple sound fields have long been a foundational part of the method of calculating acoustic intensity and specific acoustic impedance from two-microphone probes. This paper has provided a similar foundation for the phase and amplitude gradient estimator method (PAGE) by showing the bias errors for planar, monopolar, and dipolar sound fields. This bias error study has confirmed that the main advantage of the PAGE method is the bandwidth extension possible in these calculations for broadband fields. For the active intensity and specific acoustic impedance for the fields studied, the traditional method has increasing error as kd approaches π. On the other hand, the PAGE method does not have increasing error with increasing kd. Traditional estimates of reactive intensity do not exhibit error increasing with kd, and the PAGE method leaves the estimate unchanged.

As long as the probe is sufficiently far from the source (based on the source type and quantity of interest), the PAGE method is accurate in estimating acoustic intensity and specific acoustic impedance up to $kd = \pi$, a significant improvement in bandwidth over the traditional method. For broadband fields, if phase unwrapping is successfully applied, the method is accurate beyond $kd = \pi$, and is limited in bandwidth only by other sources of error such as scattering or a lack of coherence between the microphones. Because the PAGE method with unwrapping overcomes the restrictions of the spatial Nyquist limit, the microphones used for these calculations can be spaced farther apart than required by the traditional method, which in turn improves the estimates of intensity and impedance at low frequencies. Thus, the PAGE method can potentially extend the reliable bandwidth of these calculations on both the high and low end.

This bias error analysis of the PAGE method yields a foundation upon which future work can be built. An investigation into the optimal number and arrangement of microphones for multidimensional probes should be conducted along with an examination of how bias errors change when a center microphone is included in the probe. PAGE method performance in a wider range of applications, such as sound power calculations, standing wave fields and narrowband noise need to be evaluated. In addition, techniques, such as higher-order estimates of the gradient,[34] could be implemented to improve the estimates of the phase and pressure gradients for less smoothly varying fields.

Chapter 3

Three-microphone bias errors

3.1 Introduction

Acoustic intensity and specific acoustic impedance are vital quantities for characterization of fields and sources. The traditional method for estimation of acoustic intensity using multi-microphone probes was introduced in the 1970s.[8-11] Due to high-frequency bias errors in the finite-sum and finite-difference formulations, this method has a limited bandwidth determined by the microphone spacing. To overcome these bias errors, the Phase and Amplitude Gradient Estimator method (PAGE) has been developed.[21,32] This processing method uses the same multi-microphone probes as the traditional method, and the PAGE method has been shown experimentally to extend intensity estimation bandwidth by at least an order of magnitude for broadband sources.[23,25,47] In addition to active intensity, the method can be used to obtain multi-microphone estimates of reactive intensity and free-field specific acoustic impedance.

Analytical work for two-microphone traditional intensity estimation has been done by Fahy[11] and Thompson and Tree,[19] who report bias errors of the method in several ideal fields. Champoux and L'espérance[20] performed a similar analysis for two-microphone specific acoustic impedance estimation in the free-field. Building off this work, the analytical bias errors of the PAGE method for acoustic intensity and specific acoustic impedance have been reported by Whiting *et al.*[32] for a two-microphone probe in several ideal fields.

In this work, we seek to further develop the analytical foundation of Whiting *et al.* by extending it for a three-microphone probe in one dimension. Additionally, we seek to validate the analytical bias errors for both two and three microphones by presenting experimental data taken in a field produced by a monopole-like source. This chapter was modified from a 2018 paper published in the *Journal of the Acoustical Society of America* as an Express Letter under the title "Three-microphone probe bias errors for acoustic intensity and specific acoustic impedance."[33]

3.2 Methodology

With a three-microphone probe [depicted in Fig. 3.1(a)], both the traditional and PAGE methods use the center microphone to obtain the complex pressure p, removing the need to estimate center pressure by averaging. This method has been previously employed in the literature for the traditional method, albeit rarely.[12,13] The outer two microphones are used for estimation of the pressure gradient, from which particle velocity is estimated using Euler's equation, $\boldsymbol{u} = (j/\rho_0\omega)\nabla p$. Here, boldface represents a vector quantity, p is the frequency-dependent complex pressure, ρ_0 is the air density, and ω is the angular frequency. The estimates of active intensity and reactive intensity are $\boldsymbol{I} = \frac{1}{2}\mathrm{Re}\{p\boldsymbol{u}^*\}$ and $\boldsymbol{J} = \frac{1}{2}\mathrm{Im}\{p\boldsymbol{u}^*\}$, respectively, with * indicating complex conjugate. The estimate of specific acoustic impedance is $z = p/u_e$, with u_e indicating

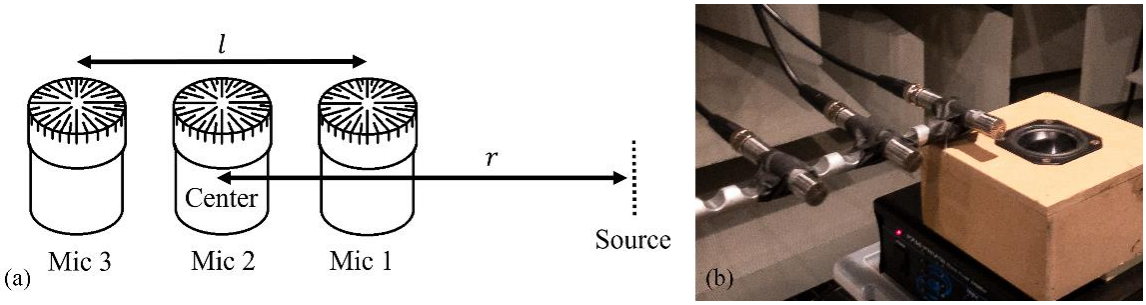

Figure 3.1. (a) Schematic of a one-dimensional intensity probe consisting of three microphones. The probe axis points towards the source, such that the sound first passes microphone 1. The

distance between the microphones is $l/2$. (b) Layout of the experiment. The three-microphone probe is shown in its closest position to the source and is moved away from the source by a scanning system. The speaker approximates a monopole source over the frequency range analyzed.

the particle velocity in the direction the specific acoustic impedance is to be measured.

The PAGE method differs from the traditional method by treating the complex pressure as an amplitude and phase, $p = Pe^{-j\phi}$. With this formulation, the PAGE formulas for active intensity, reactive intensity, and specific acoustic impedance are[32]

$$\boldsymbol{I}^{\mathrm{PAGE}} = \frac{P^2\widehat{\nabla\phi}}{2\rho_0\omega} = \frac{\bar{P}^2\widehat{\nabla\phi}}{\rho_0\omega} \tag{3.1}$$

$$\boldsymbol{J}^{\mathrm{PAGE}} = -\frac{P\,\widehat{\nabla P}}{2\rho_0\omega} = -\frac{\bar{P}\,\widehat{\nabla\bar{P}}}{\rho_0\omega} \tag{3.2}$$

$$z^{\mathrm{PAGE}} = \frac{P\rho_0\omega}{\left[P\widehat{\nabla\phi} + j\widehat{\nabla P}\right]\cdot\hat{\boldsymbol{e}}} = \frac{P^2}{2\boldsymbol{I}_c^*\cdot\hat{\boldsymbol{e}}} = \frac{\bar{P}^2}{\boldsymbol{I}_c^*\cdot\hat{\boldsymbol{e}}}, \tag{3.3}$$

where an overhat indicates an estimated quantity, $\bar{P}$ is the ensemble-averaged root-mean-square pressure amplitude at frequency ω, $\boldsymbol{I}_c$ is the complex intensity calculated as $\boldsymbol{I}_c = \boldsymbol{I} + j\boldsymbol{J}$, and $\hat{\boldsymbol{e}}$ is the direction that specific acoustic impedance is to be measured in.

In practice, $\widehat{\nabla\phi}$ is obtained via the argument of pairwise transfer functions and is therefore wrapped to be within $-\pi$ and π, which makes $\boldsymbol{I}^{\mathrm{PAGE}}$ inaccurate past the spatial Nyquist frequency, where $kl = \pi$. However, for a broadband source and with sufficient coherence between the microphones, the phase difference can be unwrapped and $\boldsymbol{I}^{\mathrm{PAGE}}$ can be accurate for $kl > \pi$. The remainder of this letter assumes that unwrapping is possible for the collected data.[25,29,32,47]

This letter reports the three-microphone bias errors of both the traditional and PAGE methods in an analytical monopole field. Additionally, any phase mismatch present in the microphones can cause low-frequency estimation errors. These can be reduced by using phase-matched microphones, performing a switching technique to calibrate phase, or by increasing the

microphone separation distance. The traditional method requires that all three microphones be well phase-matched. However, the PAGE method uses the center microphone only for pressure amplitude, eliminating the need for phase matching of the third microphone and making a PAGE-based three-microphone probe more cost effective.

To validate these analytical errors, and to compare the experimental performance between the two and three-microphone probes, bias errors were measured using a small loudspeaker approximating a monopole, as shown in Fig. 3.1(b). Three microphones were attached to a scanning system in an anechoic chamber, with the axis of the probe in line with the source and a probe length of $l = 12$ cm. Using the scanning system to move the probe, broadband noise was recorded at multiple values of r that ranged from 10 cm to 5 m.

3.3 Monopole field

In order to understand performance of the PAGE method using three microphones, the bias errors are presented in this section for estimation of active intensity, reactive intensity and specific acoustic impedance in an ideal monopole field.

The analytical bias errors depend on both the probe size relative to a wavelength, kl, and the distance from the source relative to a wavelength, kr. Here k is the acoustic wavenumber, l is the distance between outer microphones (expressed by Whiting *et al.*[32] as d for the two-microphone case), and r is the distance from the source to the probe center. It is useful to define a ratio β where $\beta = kl/kr$. As β approaches a minimum value of 0, the probe is far from the source relative to the microphone spacing, and the field becomes planar. The maximum value for β is 2, where an outer microphone overlaps the source location. In this near-field case, the sound field has significant curvature and is highly reactive, whereas in the far field, the field has nearly constant amplitude and is primarily active.

The spatially-dependent complex pressure in an ideal monopole field can be expressed as $p = Ae^{-jkr}/r$, where A is the amplitude. The analytical radial active intensity is $\boldsymbol{I} = A^2/2\rho_0 c r^2$, where c is the sound speed. Table 3.1 reports ratios of estimated-to-analytical active intensity for the two methods, for both two and three-microphone probes. These error ratios are derived by evaluating the traditional and PAGE expressions for estimation in a monopole field and dividing by the analytical quantity. The two-microphone ratios were reported previously by Whiting *et al.*[32]

Table 3.1. The estimated-to-analytical error ratios for traditional and PAGE estimation of active intensity, for both two and three-microphone probes.

Quantity	3-microphone	2-microphone
$\frac{\boldsymbol{I}^{\mathrm{TRAD}}}{\boldsymbol{I}}$	$\frac{1}{1-\beta^2/4}\mathrm{sinc}(kl/2)$	$\frac{1}{1-\beta^2/4}\mathrm{sinc}(kl)$
$\frac{\boldsymbol{I}^{\mathrm{PAGE}}}{\boldsymbol{I}}$	1	$\left(\frac{1}{1-\beta^2/4}\right)^2$

The three-microphone traditional method error level, $L_{\varepsilon,I} = 10\log_{10}\left(\left|\boldsymbol{I}^{\mathrm{TRAD}}/\boldsymbol{I}\right|\right)$, is shown in Fig. 3.2(a). This color plot (as well as the other color plots in this letter) shows the error magnitude in dB versus both kl and kr. A black diagonal line shows where $\beta = 2$, where an outer microphone overlaps the source. Lines of constant β run parallel to this line, and β is smallest towards the top left corner of the plot, where the field becomes more planar. For the traditional method, there is significant error in active intensity estimation close to the source, and the estimation error is greater than 5% for $\beta > 0.44$. For a probe length of 12 cm as in Fig. 3.1(b), this corresponds to a distance from the source to the probe center of 0.11 m. Additionally, there is error as kl increases, with more than 5% error for $kl > 1.1$, which corresponds to a frequency limit of 500 Hz for $l = 12$ cm. This is twice the bandwidth of the two-microphone case of $kl > 0.55$ [32] since the center pressure is measured and has no estimation error.

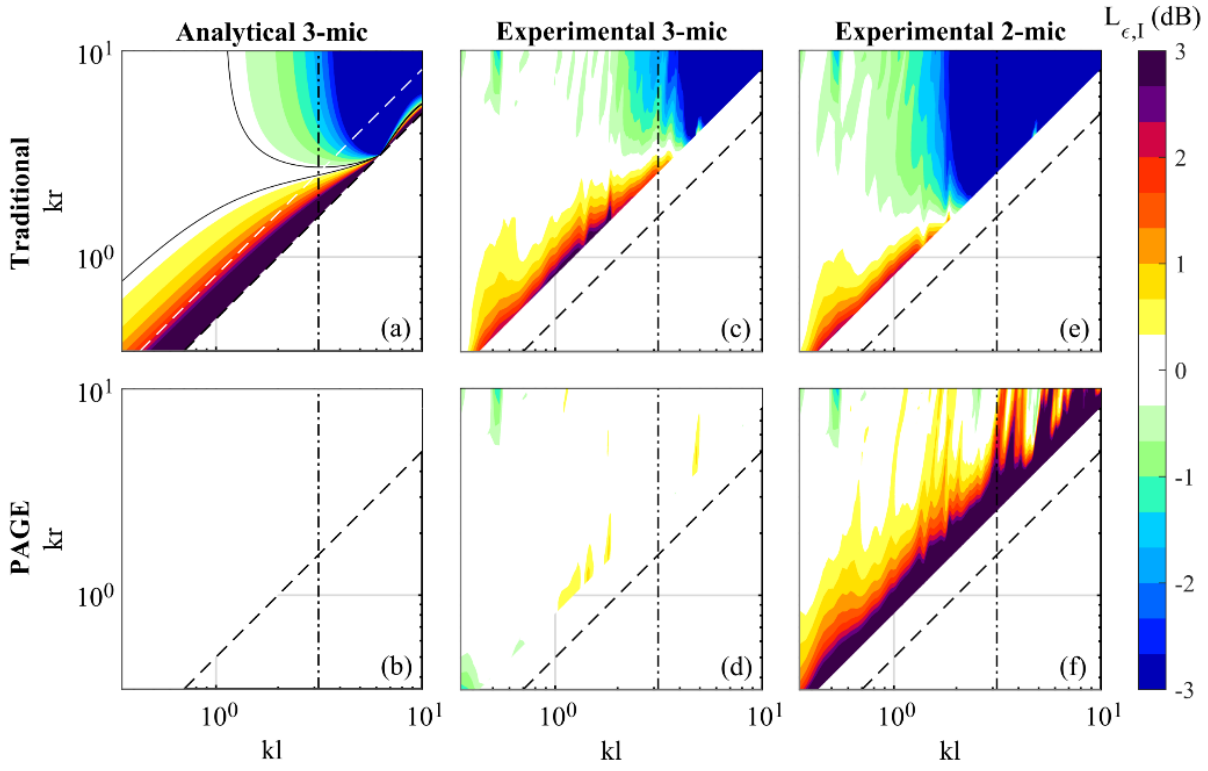

Figure 3.2. Bias errors in estimates of the magnitude of active intensity for a monopole field as a function of kl and kr: three-microphone, analytical (a) $\boldsymbol{I}^{TRAD}$ and (b) unwrapped $\boldsymbol{I}^{PAGE}$; three-microphone, experimental (c) $\boldsymbol{I}^{TRAD}$ and (d) unwrapped $\boldsymbol{I}^{PAGE}$; and two-microphone, experimental (e) $\boldsymbol{I}^{TRAD}$ and (f) unwrapped $\boldsymbol{I}^{PAGE}$. The vertical dashed line is the spatial Nyquist limit. To the left of this line, wrapped and unwrapped PAGE give the same results. The black diagonal dashed lines follow $r = l/2$. In the analytical plots, the solid black lines trace the limit of 5% error, and the white diagonal dashed line follows the closest distance to the source achievable in the experiment, for reference.

The three-microphone PAGE method results in zero bias error for active intensity in a monopole field, plotted in Fig. 3.2(b). Unlike two-microphone PAGE which has near-field error,[32] three-microphone PAGE is accurate no matter the microphone spacing or distance to the source. Therefore, of the methods considered here, three-microphone PAGE is the most accurate for active intensity estimation in a monopole field. Also, since the PAGE method uses the additional center microphone only to measure pressure amplitude, it only needs to be amplitude-calibrated and not phase calibrated.

The experimental three-microphone bias errors are shown in Figs. 3.2(c)-(d), and Figs. 3.2(e)-(f) show the two-microphone bias errors using the outer microphones, to be compared with

the analytical bias errors in Fig. 2.6. The error plotted is the ratio between the experimental intensity estimate and the expected intensity calculated from the measured center pressure, on a log scale as in Figs 3.2(a)-(b). The expected intensity in a monopole field is $\boldsymbol{I} = P^2/2\rho_0 c$. For both probes, the traditional method shows near-field error and high-frequency error as expected. By using three-microphone PAGE, both the distance requirement and the upper-frequency limit vanish. This is an improvement over two-microphone PAGE, which has significant near-field error.

Another quantity of interest is reactive intensity, which in a monopole field is $\boldsymbol{J} = A^2/2\rho_0 ckr^3$. Unlike the two-microphone case where the traditional and PAGE estimations of reactive intensity are equivalent,[32] the three-microphone estimates are different for the two methods. The estimated to analytical error ratios are reported in Table 3.2, calculated from the expressions for traditional and PAGE estimation of reactive intensity.

Table 3.2. The estimated to analytical error ratios for traditional and PAGE estimation of reactive intensity, for both two and three-microphone probes.

Quantity	3-microphone	2-microphone
$\frac{\boldsymbol{J}^{\mathrm{TRAD}}}{\boldsymbol{J}}$	$\frac{1}{1-\beta^2/4}\cos(kl/2)$	$\left(\frac{1}{1-\beta^2/4}\right)^2$
$\frac{\boldsymbol{J}^{\mathrm{PAGE}}}{\boldsymbol{J}}$	$\frac{1}{1-\beta^2/4}$	$\left(\frac{1}{1-\beta^2/4}\right)^2$

The analytical error ratio, $L_{\varepsilon,J} = 10\log_{10}\left(\left|\boldsymbol{J}^{\mathrm{TRAD}}/\boldsymbol{J}\right|\right)$, is plotted in Fig. 3.3(a). Similar to active intensity, traditional reactive intensity estimates have errors both in the near-field and for large kl. For small values of kl, the three-microphone probe has less than 5% error for $\beta < 0.44$, which is better than the two-microphone probe with the constraint $\beta < 0.31$.[32] However, the three-microphone probe also requires $kl < 0.64$ due to errors in the cross-spectral terms.

The analytical PAGE error level is plotted in Fig. 3.3(b). Three-microphone PAGE outperforms two-microphone PAGE for all values of kl, with less than 5% error for $\beta < 0.44$ as opposed to $\beta < 0.31$.[32] Also, three-microphone PAGE outperforms three-microphone traditional at high values of kl.

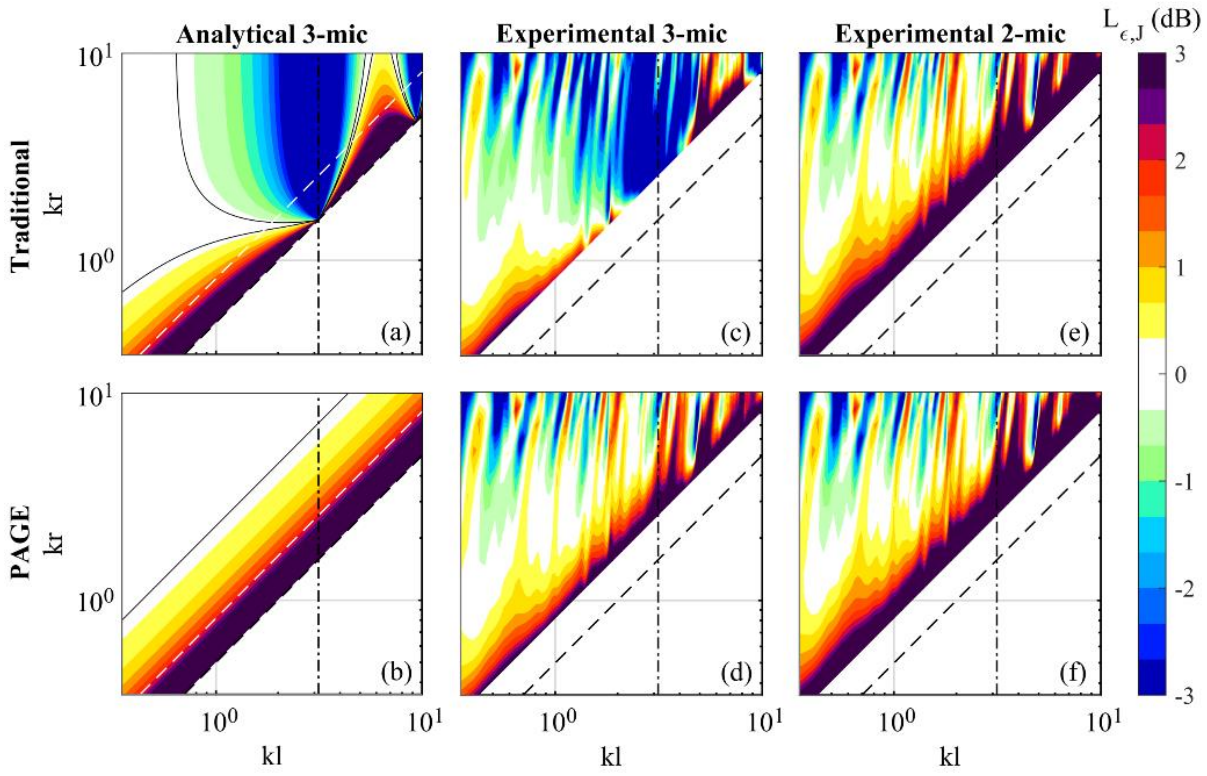

Figure 3.3. Similar to Fig. 3.2, except for the reactive intensity, $\boldsymbol{J}$.

Experimental data for reactive intensity are plotted in Figs. 3.3(c)-(f), showing error from the expected reactive intensity of $\boldsymbol{J} = P^2/2\rho_0 ckr$. The three-microphone data is compared with the analytical results shown in Fig. 3.3(a)-(b). The near-field behavior matches the analytical errors, and the traditional method shows the correct trend of increasing error as kl approaches π. The two-microphone data also shows correct trends, matching the analytical results shown in Fig. 2.7. However, for all cases, large estimation errors occur at far distances as the field becomes more

planar (active). For example, $\boldsymbol{J}$ is an order of magnitude smaller than $\boldsymbol{I}$ at the plot limit of $kr = 10$. For these small values, the estimation accuracy is limited by signal-to-noise ratio and scattering.

The final quantity explored here is specific acoustic impedance, which in a monopole field is $z = \rho_0 ckr/(kr - j)$. Table 3.3 reports the estimated to analytical error ratios, calculated from the expressions for traditional and PAGE estimation of specific acoustic impedance.

Table 3.3. The estimated to analytical error ratios for traditional and PAGE estimation of specific acoustic impedance, for both two and three-microphone probes.

Quantity	3-microphone	2-microphone
$\frac{z^{\mathrm{TRAD}}}{z}$	$\frac{\beta(1-\beta^2/4)(1+jkr)}{\beta\cos(kl/2)+2j\sin(kl/2)}$	$\beta\frac{(1+jkr)[2\cos(kd/2)+j\beta\sin(kd/2)]}{2[\beta\cos(kd/2)+j2\sin(kd/2)]}$
$\frac{z^{\mathrm{PAGE}}}{z}$	$\frac{kr-j}{kr-j/(1-\beta^2/4)}$	1

Figure 3.4(a) shows the traditional error level, $L_{\varepsilon,z} = 20\log_{10}\left(\left|z^{\mathrm{TRAD}}/z\right|\right)$, Fig. 3.4(b) shows the PAGE error level, and Figs. 3.4(c)-(f) show the experimental data, to be compared with analytical results shown in Fig. 3.4(a)-(b) and in Fig. 2.8. The experimental data shows error from the analytical value, which depends on r. The analytical three-microphone traditional method shows an improved high-frequency limit of $kl < 1.08$ over two-microphone traditional with $kl < 0.77$. On the other hand, the three-microphone PAGE method has no high-frequency limit. However, both methods have a near-field limit of $\beta > 0.44$, as opposed to the two-microphone case with no near-field limit for either method. Because two-microphone PAGE has zero bias error, it is preferred over three-microphone PAGE for specific acoustic impedance. The experimental data in Fig. 3.4(f) match these trends. Figure 3.4(e) is corrected from a previously published version of the plot[33] that didn't plot the sign of the error correctly.

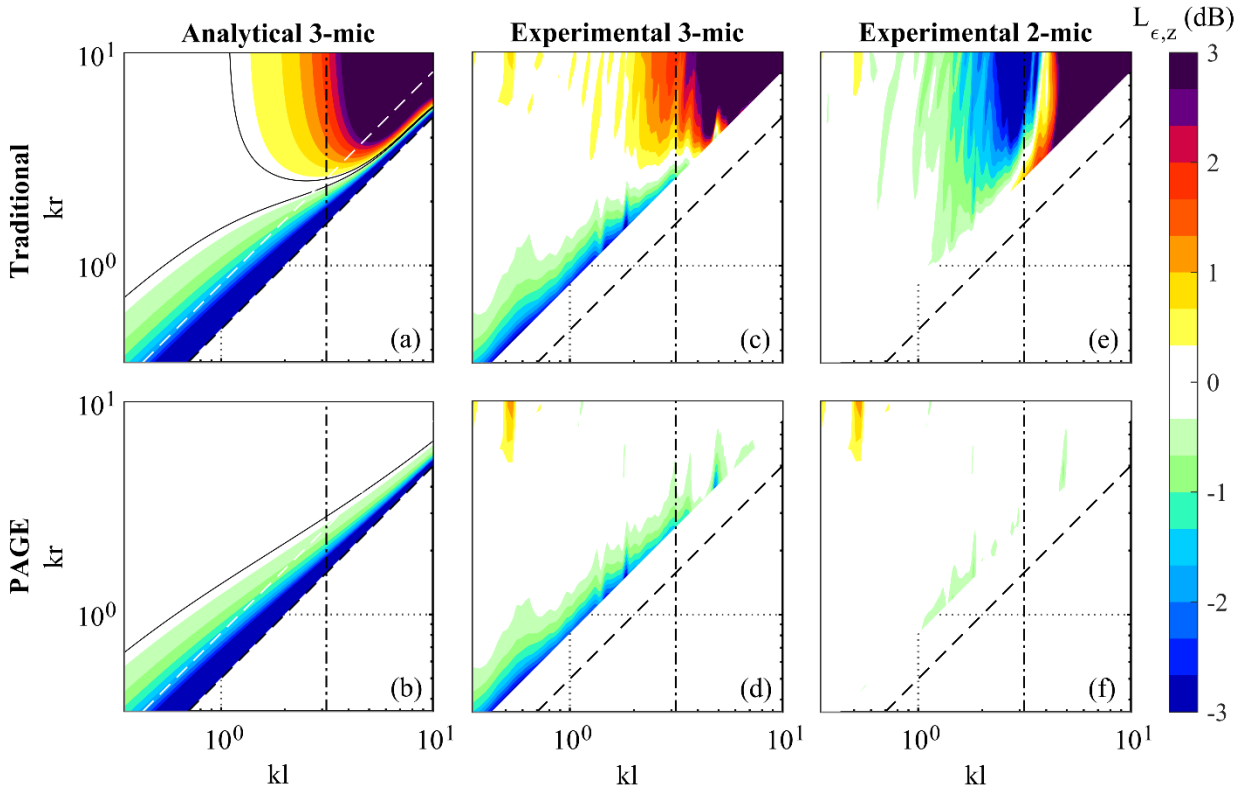

Figure 3.4. Similar to Fig. 3.2, except for the specific acoustic impedance, z.

3.4 Conclusion

In this letter, the theoretical foundation of the PAGE method has been extended by presenting monopole bias errors for a three-microphone probe for three quantities: active intensity, reactive intensity, specific acoustic impedance. To validate these bias errors, and to make an experimental comparison with the two-microphone bias errors reported by Whiting *et al.*,[32] bias errors were obtained using a small loudspeaker to approximate a monopole.

The analytical and experimental results support the following findings. First, the accuracy of active intensity estimates is significantly improved by adding a center microphone, removing error in center pressure estimation. The bandwidth of traditional method active intensity is twice that of using two microphones. Second, the three-microphone PAGE method has zero error in active intensity estimation up to the spatial Nyquist frequency, regardless of probe size or distance

to the source. For broadband sources and with sufficient coherence between the microphones, the phase can be unwrapped, which can extend the bandwidth to be an order of magnitude greater than that of the traditional method.[23] Third, the PAGE method does not require the center microphone to be phase-matched with the other microphones, so three-microphone PAGE is the most accurate of the discussed methods with no loss of feasibility other than obtaining an amplitude-calibrated center microphone. Fourth, calculation of reactive intensity with three-microphone PAGE is improved over the two-microphone methods. Finally, the three-microphone PAGE method introduces error to specific acoustic impedance estimates, so this quantity is best estimated using a probe's outer two microphones. Future work may include consideration of multi-dimensional probes, and higher-order estimation of gradients.[34]

Chapter 4

Higher-order estimation

4.1 Introduction

Obtaining accurate estimates of acoustic intensity is vital for intensity-based sound power measurements, as well as source characterization and location. A method for estimating intensity using two microphones and their cross-spectra was developed in the 1970s and is still in use today.[8-11] This method, referred to in this article as the traditional method, has a limited bandwidth highly dependent on microphone spacing. At high frequencies, when the distance between the microphones becomes large compared to a wavelength, the method has inherent bias errors due to inaccuracies in the finite-difference and finite-sum formulas.[19] On the other hand, phase mismatch of non-ideal microphones causes error when the microphone spacing is small compared to a wavelength, at low frequencies. These two constraints limit the estimation bandwidth of a two-microphone intensity probe.

In order to overcome the high-frequency bias errors and extend estimation bandwidth, the Phase and Amplitude Gradient Estimator method (PAGE) has been developed.[21] By separating the frequency-dependent complex pressures into amplitude and phase, calculations of active and reactive intensity take a new form. The PAGE method has extended the bandwidth of plane wave measurements by at least an order of magnitude for broadband sources.[23]

For an ideal plane wave, the PAGE method estimation of active and reactive intensity has zero bias errors at higher frequencies.[28] Thus, the remaining error is the low-frequency phase

mismatch error, which occurs as the probe spacing is small relative to a wavelength. Therefore, probes with larger microphone separation are preferred over probes with smaller separation. However, with a larger probe, it can be harder for the PAGE method to function accurately in non-planar fields, such as a monopole field or a standing wave field. In this work, we explore how the use of additional microphones and higher-order estimates of the first derivatives can improve intensity estimation accuracy in these high-curvature fields. This chapter was modified from a 2017 publication in *Proceedings of Meetings on Acoustics* under the title "Higher-order estimation of active and reactive acoustic intensity."[34]

4.2 Methodology

The multiple-microphone approach to estimating intensity has been explored by Cazzalato and Hansen[12] and Pascal and Li.[13] Under these formulations, gradients are estimated using a least-squares method across the microphones. This traditional method can be extended with the PAGE formulation resulting in a process referred to as least-squares PAGE.

An overview of the traditional and PAGE methods is given here. The general formulas for frequency-domain calculations of active and reactive intensity are

$$\boldsymbol{I} = \frac{1}{2} Re\{p\boldsymbol{u}^*\} \tag{4.1}$$

$$\boldsymbol{J} = \frac{1}{2} Im\{p\boldsymbol{u}^*\} \tag{4.2}$$

where p is the complex pressure at the center of the probe, $\boldsymbol{u}$ is the complex particle velocity, and $*$ denotes a complex conjugate. In the traditional method, p is either obtained from a microphone at the center of the probe or estimated as a weighted average from multiple microphones at surrounding locations. These weights are determined for the probe configuration either according

to a least-squares estimation scheme or by using the higher-order method that will be explained later in this article. The traditional method estimates particle velocity using Euler's equation,

$$\boldsymbol{u}^{TRAD} = \frac{j}{\rho_0 \omega} \widehat{\nabla p}, \tag{4.3}$$

where ρ_0 is the ambient air density, ω is the angular frequency, and an overhat indicates that the quantity is estimated. The estimated gradient of the complex pressure, $\widehat{\nabla p}$, comes from a finite-difference between the probe microphones. In the traditional method, the complex forms of p and $\boldsymbol{u}^{TRAD}$ are used in Eqs. (4.1) and (4.2) to estimate active and reactive intensity.

The PAGE method, on the other hand, treats complex pressure not in terms of real and imaginary parts, but as amplitude and phase, where $p = Pe^{-j\phi}$. The amplitude of the pressure at the center of the probe, P, is either measured by a microphone at the center of the probe or estimated as a weighted average of the amplitudes of the outer microphones. The PAGE equations for active and reactive intensity are[21]

$$\boldsymbol{I}^{PAGE} = \frac{\hat{P}^2 \widehat{\nabla \phi}}{2\rho_0 \omega} \tag{4.4}$$

and

$$\boldsymbol{J}^{PAGE} = -\frac{\hat{P}\, \widehat{\nabla P}}{2\rho_0 \omega}. \tag{4.5}$$

The estimate of the gradient of the phase across the probe, $\widehat{\nabla \phi}$, is obtained via the phase of the transfer functions between microphone pairs. In a plane wave field, the PAGE formulation for active and reactive intensity has zero bias errors up to the spatial Nyquist frequency. If the source is broadband, and there is sufficient coherence between the microphones, a transfer function's phase can be unwrapped, allowing an estimate of active intensity to be accurate above the spatial Nyquist frequency. The success of the PAGE method in extending the bandwidth of reliable

intensity estimates has been shown for propagating (active) sound fields.[23] However, performance of the PAGE method in standing wave (reactive) sound fields has been relatively unexplored.

To hopefully obtain more accurate intensity estimates in reactive sound fields, the higher-order PAGE method has been developed, following the work of Jensen.[48] This allows for higher-order estimation of $\hat{P}$, $\widehat{\nabla P}$, and $\widehat{\nabla \phi}$, which are needed for $\boldsymbol{I}^{\mathrm{PAGE}}$ and $\boldsymbol{J}^{\mathrm{PAGE}}$. In his work, Jensen developed a method to obtain higher-order estimates of a function and its derivatives using an arbitrary grid of measurement points. Following Jensen's notation, the function f (which could represent either P or ϕ) is sampled at several measurement positions each as g_i, where i is the index of the grid position. Each value of g_i can be expressed as a linear combination of f and its derivatives evaluated at the origin, according to the Taylor series expansion. In two dimensions, g_i can be expressed as

$$\begin{aligned} g_i &\equiv f(\alpha_i, \beta_i) \\ &= f(0,0) + \left(\alpha_i \frac{\partial}{\partial x} + \beta_i \frac{\partial}{\partial y}\right) f(0,0) + \cdots + \left(\alpha_i \frac{\partial}{\partial x} + \beta_i \frac{\partial}{\partial y}\right)^m f(0,0) \frac{1}{m!} - \delta_i \end{aligned} \tag{4.6}$$

where α_i and β_i are the x and y coordinates, respectively, of grid position i relative to the origin, m is the desired accuracy order, and δ_i is an error constant of order $m+1$. The origin can be defined arbitrarily, although it is usually placed at the center of the probe. Equation (4.6) can be written in matrix form to include all the grid positions as

$$T_m F_m = G_m + \varepsilon_m. \tag{4.7}$$

The vector F_m contains the derivatives in the Taylor series (along with their appropriate factorial coefficients):

$$F_m = \left(f \;\; \frac{\partial f}{\partial x} \;\; \cdots \;\; \frac{1}{i!} \frac{\partial^i f}{\partial x^{i-j} \partial y^j} \;\; \cdots \;\; \frac{1}{m!} \frac{\partial^m f}{\partial y^m} \right)^T, \tag{4.8}$$

where T denotes a vector transpose. The matrix T_m contains a row for each grid position, where each row consists of the grid coordinates raised to appropriate powers matching the Taylor series derivatives in F_m,

$$T_m = \begin{bmatrix} 1 & \alpha_1 & \beta_1 & {\alpha_1}^2 & 2\alpha_1\beta_1 & \cdots & {\beta_1}^m \\ 1 & \alpha_2 & \beta_2 & {\alpha_2}^2 & 2\alpha_2\beta_2 & \cdots & {\beta_2}^m \\ \vdots & \vdots & \vdots & \vdots & \vdots & \ddots & \vdots \\ 1 & \alpha_{n_m} & \beta_{n_m} & {\alpha_{n_m}}^2 & 2\alpha_{n_m}\beta_{n_m} & \cdots & {\beta_{n_m}}^m \end{bmatrix}, \tag{4.9}$$

and n_m is the number of grid positions. If F_m includes all the derivatives in the two-dimensional Taylor series, then the number of grid positions needed to achieve the desired accuracy order, m, is

$$n_m = (m+1)(m+2)/2. \tag{4.10}$$

The right side of Eq. (4.7) consists of a vector of the grid measurements

$$G_m = \begin{pmatrix} g_1 & g_2 & \cdots & g_{n_m} \end{pmatrix}^T \tag{4.11}$$

and an error vector

$$\varepsilon_m = \begin{pmatrix} \delta_1 & \delta_2 & \cdots & \delta_{n_m} \end{pmatrix}^T. \tag{4.12}$$

Estimates of the function f and its derivatives, evaluated at the origin, are found by solving Eq. (4.7) for F_m,

$$F_m = {T_m}^{-1} G_m + E_m \tag{4.13}$$

where E_m is an unknown error vector of order $m+1$,

$$E_m = {T_m}^{-1} \varepsilon_m. \tag{4.14}$$

Because the error vector E_m is unknown, the accuracy order of estimates in Eq. (4.13) is m, the order of the terms used in the Taylor series. For any probe geometry, the rows of ${T_m}^{-1}$ give sets of finite difference coefficients that, when combined with the quantities measured at the grid locations, calculate the function f and its derivatives evaluated at the origin. Once these finite

difference coefficients are obtained, they can be reused for any data set, provided the probe geometry and estimation location remain constant.

In order to estimate active and reactive intensity using the PAGE method [Eqs. (4.4)–(4.5)], $\hat{P}$, $\widehat{\nabla P}$, and $\widehat{\nabla \phi}$ are needed. $\hat{P}$ and $\widehat{\nabla P}$ can be obtained by following the above procedure with measurements of P at each microphone making up G_m. Since phase is a quantity wrapped between $-\pi$ and π, measurements of ϕ at each microphone are not absolute phases, and cannot be used to accurately obtain $\widehat{\nabla \phi}$. To circumvent this issue, one microphone is chosen as a reference microphone, and relative phases are obtained at each microphone by unwrapping the phase of the transfer function relative to the reference microphone. These relative phases can be used in G_m to obtain $\widehat{\nabla \phi}$. It is often preferable to calculate the transfer function relative to a center microphone to minimize distances between microphone pairs, as this minimizes unwrapping errors.

By choosing which derivatives to include in F_m, as well as the corresponding coordinates in T_m, the higher-order method for estimating f can be employed for one, two, or three dimensions. However, the matrix T_m must be non-singular or the inverse cannot be obtained. For example, if the three-dimensional Taylor series is used, the grid points cannot lie in a line or in a plane. The impact of including higher-order estimates of $\hat{P}$, $\widehat{\nabla P}$, and $\widehat{\nabla \phi}$ in the PAGE method are now discussed for the case of a one-dimensional probe near a monopole and in a standing wave field, followed by an examination of how to apply this technique for two-dimensional probes.

4.3 Monopole

In order to understand how higher-order PAGE performs in a field with curvature, we have analyzed the method's performance for active intensity estimation in a monopole field. Figure 4.1 shows three one-dimensional probes used in this simulated field, consisting of two, four, and six

microphones evenly spaced along a line pointing to the source, where d is the distance between microphones and r is the distance from the center of the probe to the source.

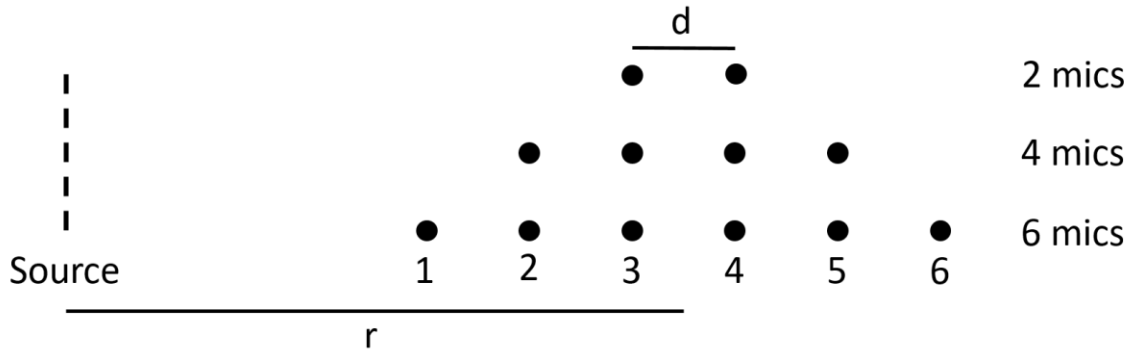

Figure 4.1. Schematic of one-dimensional probes consisting of two, four and six microphones. The distance between microphones is d, and the distance from the center of the probe to the source is r.

PAGE estimation of active intensity [Eq. (4.4)] relies on $\hat{P}$ and $\widehat{\nabla\phi}$, which are both estimated using the higher-order method. To illustrate how the higher-order method functions in this case, the following three equations show how $\widehat{\nabla\phi}$ is obtained using two, four, and six microphones, respectively:

$$\widehat{\nabla\phi} = \frac{1}{d}(-\phi_3 + \phi_4) \tag{4.15}$$

$$\widehat{\nabla\phi} = \frac{1}{d}\left(\frac{1}{24}\phi_2 - \frac{9}{8}\phi_3 + \frac{9}{8}\phi_4 - \frac{1}{24}\phi_5\right) \tag{4.16}$$

$$\widehat{\nabla\phi} = \frac{1}{d}\left(-\frac{3}{640}\phi_1 + \frac{25}{384}\phi_2 - \frac{75}{64}\phi_3 + \frac{75}{64}\phi_4 - \frac{25}{384}\phi_5 + \frac{3}{640}\phi_6\right) \tag{4.17}$$

In practice, each phase ϕ is the phase of an unwrapped transfer function relative to one of the microphones. Similar equations exist to estimate P with different coefficients, although they are not shown here.

The bias errors in active intensity in a simulated monopole field for two, four and six microphones, shown in Figure 4.2, illustrate the effect of higher-order PAGE. When the PAGE method with unwrapping is used, these errors are independent of frequency. Each of the probes

has large error as one of the outer microphones approaches the source, which happens at a larger value of r/d for more microphones due to the larger probe size. However, since having more microphones allows for better sampling of the sound field, the bias error converges to zero faster. As the probe moves away from the source, the 4-microphone probe is the first to achieve less than 0.2 dB error at $r/d = 2.15$. The 2-microphone probe does not achieve less than 0.2 dB error until $r/d = 3.31$, making use of the 4-microphone probe advantageous over that range in the near-field. The six-microphone probe achieves less than 0.2 dB error at $r/d = 2.98$, which, due to the large size of the probe, is farther from the source than the four-microphone probe. Thus, the 4-microphone probe is generally preferable, achieving less than 0.2 dB error at the closest distance to the source.

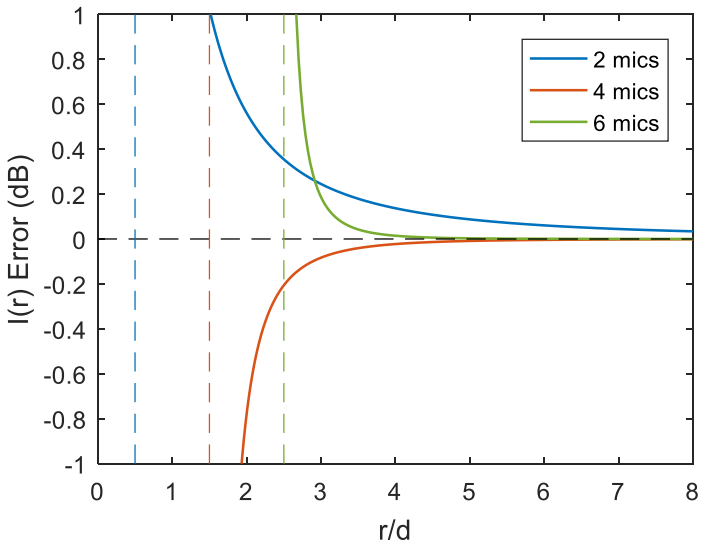

Figure 4.2. Active intensity error in a simulated monopole field for one-dimensional probes consisting of two, four and six microphones. The three dashed vertical lines correspond to values of r/d for each probe where an outer microphone is at the source.

4.4 Standing wave

The performance of higher-order PAGE is further evaluated by considering a standing wave field, which is purely reactive. Figure 4.3(a) shows performance of the higher-order PAGE

method reactive intensity estimation for probes consisting of two, four and six microphones in a simulated standing wave versus kd. The probe center for all three probes is placed at a point of maximum reactive intensity, halfway between a pressure node and a pressure antinode. Probes with higher numbers of microphones perform better; however, this benefit is reduced at high values of kd when the probe becomes large enough to span a null. As a purely real field, the complex pressure is either positive or negative, alternating across nulls. Since the PAGE expressions involve only the magnitude of the pressure, the entire field has positive amplitude under this method, interfering with the estimate of center pressure when the probe spans a null. PAGE with two microphones is within 0.2 dB error for $kd < 0.56$, whereas higher-order PAGE with six microphones is within 0.2 dB error for $kd < 0.97$, nearly doubling the frequency range of accurate reactive intensity estimation.

To compare with higher-order PAGE, the higher-order formulation in Sec. 4.2 can also be used to develop a higher-order traditional method. The higher-order traditional calculation uses the methods explained in Sec. 4.2 to estimate the complex pressure and its gradient, rather than estimating pressure amplitude and phase gradients as in the PAGE method. The performance of the higher-order traditional method for estimating reactive intensity in the same standing wave field is shown in Figure 4.3(b). The two-microphone traditional method result is identical to the two-microphone PAGE calculation because both calculations depend on a difference of autospectra.[32] However, the higher-order traditional method outperforms higher-order PAGE for reactive intensity in a standing wave field, with less than 0.2 dB error for $kd < 1.54$ for the six microphone probe, which is closer to the spatial Nyquist limit of $kd = \pi$ than the higher-order PAGE estimate. By using the higher-order traditional method with six microphones, the frequency

range of accurate reactive intensity estimation in a standing wave field is nearly three times that of using two microphones.

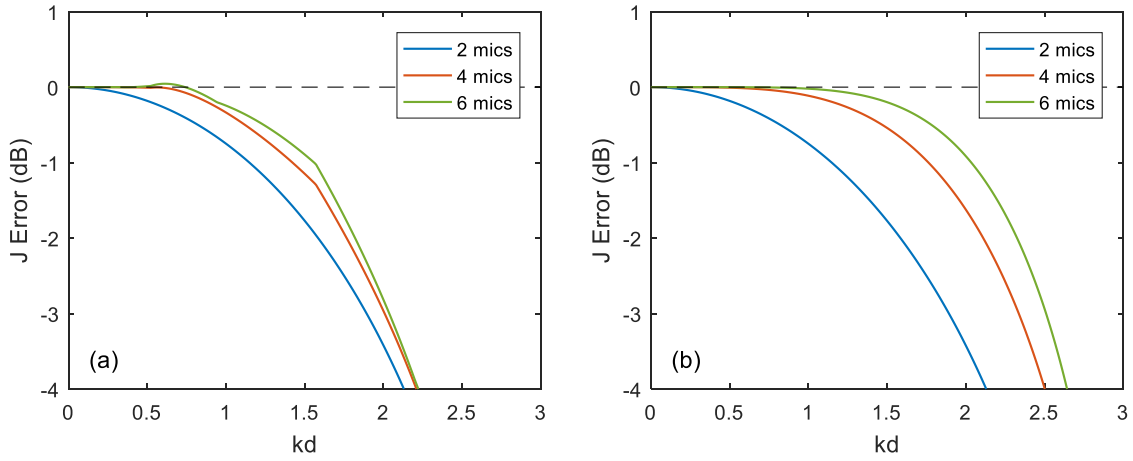

Figure 4.3. Reactive intensity error in a simulated standing wave field using (a) higher-order PAGE and (b) higher-order traditional. The probe center is halfway between a pressure node and a pressure antinode.

4.5 Two-dimensional probe

The higher-order method can be extended to two and three-dimensional probes. As an example, Fig. 4.4 shows a two-dimensional probe used in several applications.[22,23,25] This probe consists of microphones in an equilateral triangle with a fourth microphone at the centroid.

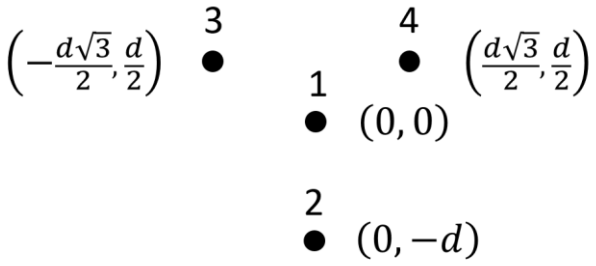

Figure 4.4. A two-dimensional intensity probe. Each microphone is labeled with a microphone number and its (x, y) coordinates, where d is the distance from each outer microphone to the center microphone.

For this probe, intensity estimation differs between the least-squares and higher-order PAGE methods. In both methods, pressure is obtained directly by the center microphone. Both

methods estimate the x-component of the gradients using a difference of microphones 4 and 3. The methods differ in estimating the y-component of the gradients. The least-squares estimate of the y-component of $\nabla\phi$ is

$$\frac{\partial\phi}{\partial y} = \frac{1}{d}\left(-\frac{2}{3}\phi_2 + \frac{1}{3}\phi_3 + \frac{1}{3}\phi_4\right). \tag{4.18}$$

Again, in practice each value of ϕ is the unwrapped phase of a transfer function relative to one of the microphones. The higher-order estimate is

$$\frac{\partial\phi}{\partial y} = \frac{1}{d}\left(-\phi_1 - \frac{1}{3}\phi_2 + \frac{2}{3}\phi_3 + \frac{2}{3}\phi_4\right). \tag{4.19}$$

The higher-order PAGE estimate shown in Eq. (4.19) uses all four microphones instead of three, providing a higher-order of accuracy. Additionally, the higher-order method centers the y component of the gradient correctly at the origin. The least-squares method centers the estimate at $(0, -d/4)$, which means that the pressure and the particle velocity estimate are not collocated, causing error in the intensity estimate. The usefulness of higher-order PAGE in extending the bandwidth needs to be experimentally verified.

4.6 Conclusion

The method described in this paper can be used to obtain higher-order intensity estimates from probes in one, two, and three-dimensions, given a sufficient number of microphones. Both the traditional and the PAGE methods can benefit, in certain cases, from the higher-order estimates presented in this paper. The higher-order processing can be utilized with currently existing probes, as well as guide the creation of new probe designs.

The higher-order method can improve accuracy of active intensity estimation; however, the efficacy of higher-order estimation is of particular interest in reactive sound fields. In a monopole case, estimation of active intensity using four microphones and the higher-order PAGE

method is within 0.2 dB error for distances closer to the monopole than using two microphones with the least-squares PAGE method. For reactive intensity in a standing wave field, using six microphones with the higher-order PAGE method is more accurate, but using six microphones with the higher-order traditional method extends the frequency range over which error is less than 0.2 dB even further, by nearly three times the two-microphone result. Future work may include investigation of more complicated analytical fields, experimental validation of bias errors, and considerations of additional probe designs.

Chapter 5

Directional pressure

5.1 Introduction

Directional pressure sensors have a variety of uses, including direction finding, energy-based quantity estimation, and source discrimination. One common approach is pressure gradient sensing using a microphone array, such as in the case of a cardioid microphone.[49-51] Pressure gradient sensors serve as a basis for intensity estimation, and can be extended to create higher-order sensors such as a particle velocity gradient sensor.[52-55] Another approach is beamforming, using time (or phase) delays to steer a microphone array in arbitrary directions.[56,57] Several more complicated methods of directional sensing exist.[58-62]

Recently, the phase and amplitude gradient estimator (PAGE) method has been developed,[21] which relies on the phase gradient to accurately estimate acoustic vector intensity up to the spatial Nyquist frequency for propagating fields. For broadband sources and with sufficient coherence between the microphones,[29] the phase gradient can be unwrapped,[23] allowing the method to be accurate at frequencies much higher than the spatial Nyquist frequency.[32] In this letter, we report a directional pressure method similar to particle velocity gradient sensing, utilizing the phase gradient to increase both the directionality and the bandwidth of frequency-dependent source localization using two microphones. This chapter was modified from a paper submitted for publication in the *Journal of the Acoustical Society of America* as an Express Letter under the title "Highly directional pressure sensing using the phase gradient."

5.2 Theory

As shown by Bastyr,[52] the continuity equation can be used to estimate pressure using spatial derivatives of the particle velocity. This estimate can be combined with particle velocity to create a u-u intensity sensor, or used alone as a directional pressure sensor as done by de Bree and Wind.[53] For a time-harmonic process with $e^{j\omega t}$ dependence, complex pressure relates to the divergence of the particle velocity as

$$p = \frac{j\rho_0 c^2}{\omega} \nabla \cdot \boldsymbol{u}, \tag{5.1}$$

where ρ_0 is the air density, c is the sound speed, ω is the angular frequency, $\boldsymbol{u}$ is the particle velocity, and $j = \sqrt{-1}$. In Cartesian coordinates, the divergence in Eq. (5.1) is separated into three components, expressing the complex pressure as a summation:

$$p = \frac{j\rho_0 c^2}{\omega} \left[\frac{\partial u_x}{\partial x} + \frac{\partial u_y}{\partial y} + \frac{\partial u_z}{\partial z} \right]. \tag{5.2}$$

In the far field of a source, the three derivative terms in Eq. (5.2) each represent sound pressure corresponding with particle motion in a single direction. Pressure from a single direction can be evaluated with a one-dimensional array, used to estimate a single derivative from Eq. (5.2):

$$p_x = \frac{j\rho_0 c^2}{\omega} \frac{\partial u_x}{\partial x}, \tag{5.3}$$

where x is the direction along the array axis. This directional pressure quantity can be estimated using two particle velocity sensors and a finite difference. Alternatively, since particle velocity can be related to the pressure gradient through the time-harmonic Euler equation, the directional pressure in Eq. (5.3) can be obtained using three microphones in a line to estimate a second derivative of pressure. The directivity associated with these derivatives produces a $\cos^2\theta$ array response.

In estimating Eq. (5.3) using multiple sensors, finite-difference errors cause high-frequency inaccuracy, as the wavelength becomes small relative to the microphone separation.[32] The PAGE method was developed to remove such errors in frequency-domain active intensity. By expressing pressure as an amplitude and a phase, $p = Pe^{-j\phi}$, Euler's equation for particle velocity takes a new form that relies on the unwrapped phase gradient, and is expressed as

$$\boldsymbol{u} = \frac{e^{-j\phi}}{\rho_0 \omega}(P\,\nabla\phi + j\nabla P). \tag{5.4}$$

Use of Eq. (5.4) as opposed to the gradient of complex pressure removes finite difference error for plane waves up to the spatial Nyquist frequency.[32] Additionally, the method can produce accurate gradient estimates beyond the spatial Nyquist frequency for broadband sources when phase unwrapping can properly be applied.[23]

By substituting Eq. (5.4) into Eq. (5.3), the contribution to pressure in the direction of the array axis can be expressed in terms of P and ϕ as

$$p_x = \frac{1}{k^2}\left[jP\frac{\partial^2\phi}{\partial x^2} + 2j\frac{\partial P}{\partial x}\frac{\partial \phi}{\partial x} - \frac{\partial^2 P}{\partial x^2} + P\left(\frac{\partial \phi}{\partial x}\right)^2\right]e^{-j\phi}, \tag{5.5}$$

where $k = \omega/c$ is the acoustic wavenumber. Each of the phase derivatives in Eq. (5.5) can be estimated using the phase of transfer functions between microphones, removing finite-difference error and extending bandwidth up to the spatial Nyquist frequency, and even higher when the phase can be unwrapped.

To investigate the behavior of Eq. (5.5), each term can be evaluated in a monopole field. For a source at the origin, the monopole pressure field is $P = A/r = A/\sqrt{x^2 + y^2}$ and $\phi = kr = k\sqrt{x^2 + y^2}$, where A is amplitude, r is the array distance to the source, and x and y are components of r, with x being the component of r along the array axis. Partial derivatives of P

and ϕ in Eq. (5.5) are evaluated for the monopole field (for example, $\partial\phi/\partial x = kx/\sqrt{x^2+y^2} = k\cos\theta$), resulting in the response,

$$p_{x,\text{monopole}} = \frac{A}{k^2}\left[\frac{k^2}{r}\cos^2\theta + \left(\frac{jk}{r^2}+\frac{1}{r^3}\right)(\sin^2\theta - 2\cos^2\theta)\right]e^{-j\phi}. \tag{5.6}$$

This response is shown in Fig. 1(a) for several frequencies, for $r = 2.1$ m (7 ft). The first term in Eq. (5.5) results in a $\cos^2\theta$ response at all distances, represented by the first term in Eq. (5.6). The remainder of Eq. (5.6) results from the last three terms in Eq. (5.5), altering the response in the near field, with a $\sin^2\theta$ term creating a significant response when pointing perpendicular to the source ($\theta = 90°$). Therefore, using components of the divergence as done by de Bree and Wind[53] leads to ineffective direction finding in the near field.

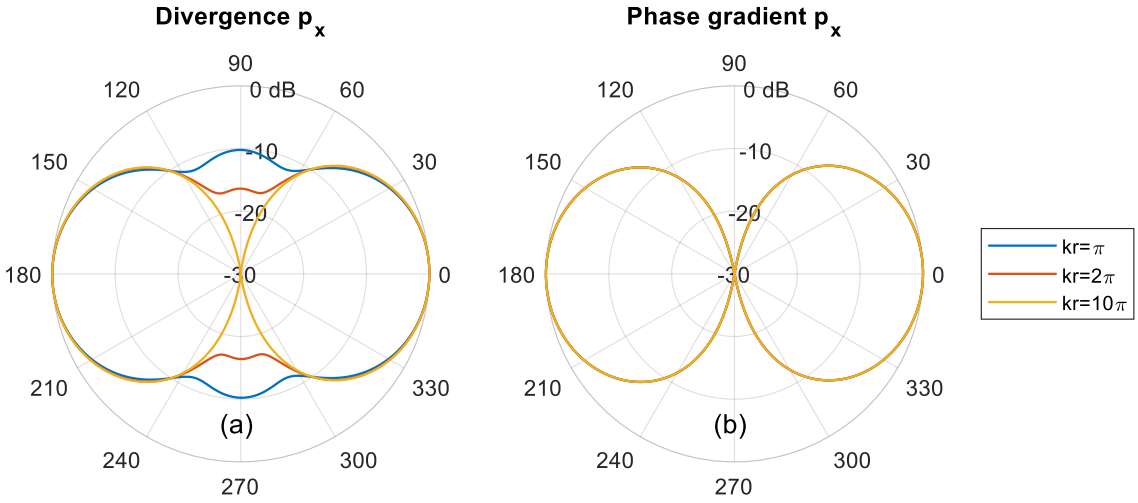

Figure 5.1. Theoretical response for (a) divergence-based [Eq.(5.5)] and (b) phase gradient-based [Eq.(5.7)] directional pressure components as a function of angle θ for several values of kr, where r is fixed to be 2.1 m (7 ft).

By assuming that the array is at least several wavelengths from the source, Eq. (5.5) can be simplified as

$$p_x = \frac{1}{k^2}\left(\frac{\partial\phi}{\partial x}\right)^2 Pe^{-j\phi}. \tag{5.7}$$

dropping the terms that altered the near-field response for a monopole. Since Eq. (5.7) contains no second derivatives, p_x can be estimated using only two microphones instead of three. Additionally, despite being a far-field limit, the simplified directional pressure in Eq. (5.7) has a $\cos^2\theta$ array response when used in either the near or the far field, as shown in Fig. 1(b).

The modified form of the particle velocity divergence sensor in Eq. (5.7) serves as the basis for calculating directional pressure using the phase gradient. In a field produced by a monopole, the magnitude of the phase gradient is $|\nabla\phi| = k$, so p can be expressed as

$$p = \frac{1}{k^2}|\nabla\phi|^2 P e^{-j\phi}. \tag{5.8}$$

The phase gradient in Eq. (5.8) can be split into its components as

$$p = \frac{1}{k^2}\left[\left(\frac{\partial\phi}{\partial x}\right)^2 + \left(\frac{\partial\phi}{\partial y}\right)^2 + \left(\frac{\partial\phi}{\partial z}\right)^2\right] P e^{-j\phi} \tag{5.9}$$

such that the complex pressure is expressed as a summation of three components in orthogonal directions. As opposed to divergence-based components in Eq. (5.2), Eq. (5.9) contains components of the phase gradient, which relate directly to the sound propagation. Since active intensity can also be expressed in terms of the phase gradient,[21] a single directional pressure component has a maximum response in the same direction as a one-dimensional intensity estimate, but with a $\cos^2\theta$ response as opposed to a $\cos\theta$ response.

An additional advantage of using phase gradient-based directional pressure is the possibility to achieve an arbitrary array response through modification of Eq. (5.7). Since the relative array response is simply a function of $(\partial\phi/\partial x)/k$, a modification of this directivity factor changes the response of the array. Several possibilities for improving array response are discussed in the remainder of this section.

A higher-order bidirectional sensor can be created to achieve an array response narrower than $\cos^2\theta$. This is done by changing the power on the directivity factor in Eq. (5.7), raising it to an arbitrary power M, resulting in

$$p_{x,M} = \frac{1}{k^M}\left(\frac{\partial\phi}{\partial x}\right)^M Pe^{-j\phi}, \tag{5.10}$$

which achieves a $\cos^M\theta$ array response with the use of only two microphones. Figure 2(a) shows the simulated response for a two-microphone directional sensor achieving a $\cos^M\theta$ response by using Eq. (5.10) with different values of M.

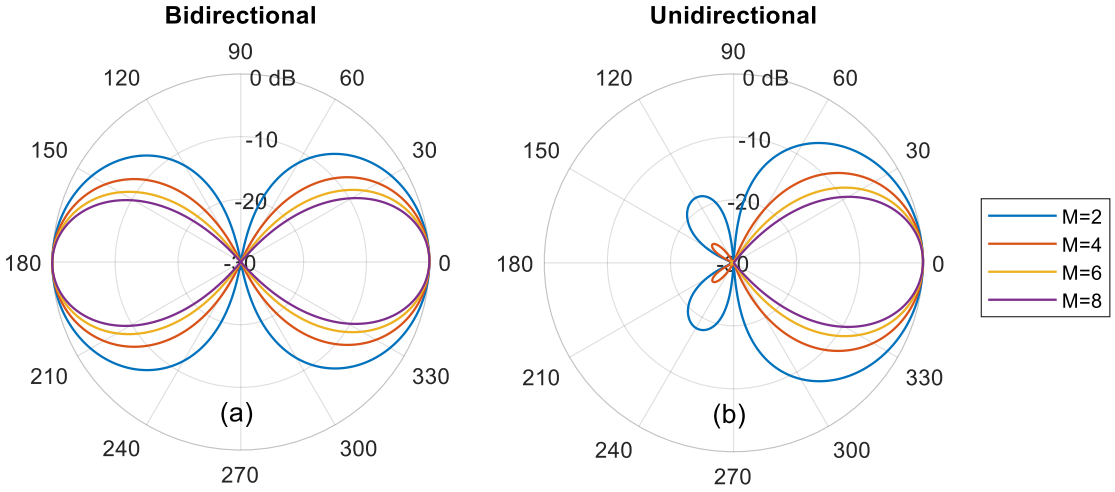

Figure 5.2. Simulated array response for (a) bidirectional [Eq.(5.9)] and (b) unidirectional sensors [Eq.(5.10)] using two microphones and the phase-gradient method, for different orders, M.

In many cases, it may be beneficial to have an array response that is unidirectional instead of bidirectional, such that the array is sensitive in one direction instead of two. This is done by further modifying the directional pressure expression, combining even and odd powers of the directivity factor from Eq. (5.10). Since odd powers of the directivity factor have a negative response in the back of the array, the array response in that direction nearly cancels when combined with an even power. The unidirectional pressure can be expressed as

$$p_{x,uni} = \frac{1}{2}\left[\frac{1}{k^M}\left(\frac{\partial\phi}{\partial x}\right)^M + \frac{1}{k^{M-1}}\left(\frac{\partial\phi}{\partial x}\right)^{M-1}\right] Pe^{-j\phi}. \quad (5.11)$$

The resulting unidirectional array response is shown in Fig. 2(b) for several values of M.

A final modification allows for computational steering of the array response. With a two-dimensional array, two components of the phase gradient can be estimated. Using both components, the direction of sensitivity is not constrained by the array axis, and the beam can be steered computationally to an arbitrary angle θ_0. For a unidirectional sensor,

$$p_{x,uni} = \frac{1}{2}\left[\frac{1}{k^M}\left(\cos\theta_0\frac{\partial\phi}{\partial x} + \sin\theta_0\frac{\partial\phi}{\partial y}\right)^M + \frac{1}{k^{M-1}}\left(\cos\theta_0\frac{\partial\phi}{\partial x} + \sin\theta_0\frac{\partial\phi}{\partial y}\right)^{M-1}\right] Pe^{-j\phi}, \quad (5.12)$$

where θ_0 is the angle from the x-axis on the x-y plane.

Using these modifications, an array response $\cos^M\theta$ can be created using two microphones. With a two-dimensional array (three or more microphones), that response can be steered to an arbitrary direction. Further manipulation of the directivity factor can lead to additional array responses, suited for a variety of purposes.

5.3 Experiment

To validate the phase gradient formulation of directional pressure, and to compare the array response with those of other methods, an experiment was performed in an anechoic chamber. A microphone array was attached to a turntable, composed of two, perpendicular microphone pairs, each with a separation, d = 10 cm (4 in). The microphones were 1.27 cm (1/2 in) free-field, condenser microphones, and each pair was phase-matched. One pair acted as a broadside array for time-domain, additive beamforming, and the other pair was used for the pressure-gradient and phase-gradient methods, sensing along the array axis. To map the array response of each two-

microphone method, the array was rotated in increments of 5° relative to a fixed loudspeaker 2.1 m (7 ft) away producing white noise. The measurement schematic and array response for several two-microphone processing methods at three frequencies are shown in the top row of Fig. 3.

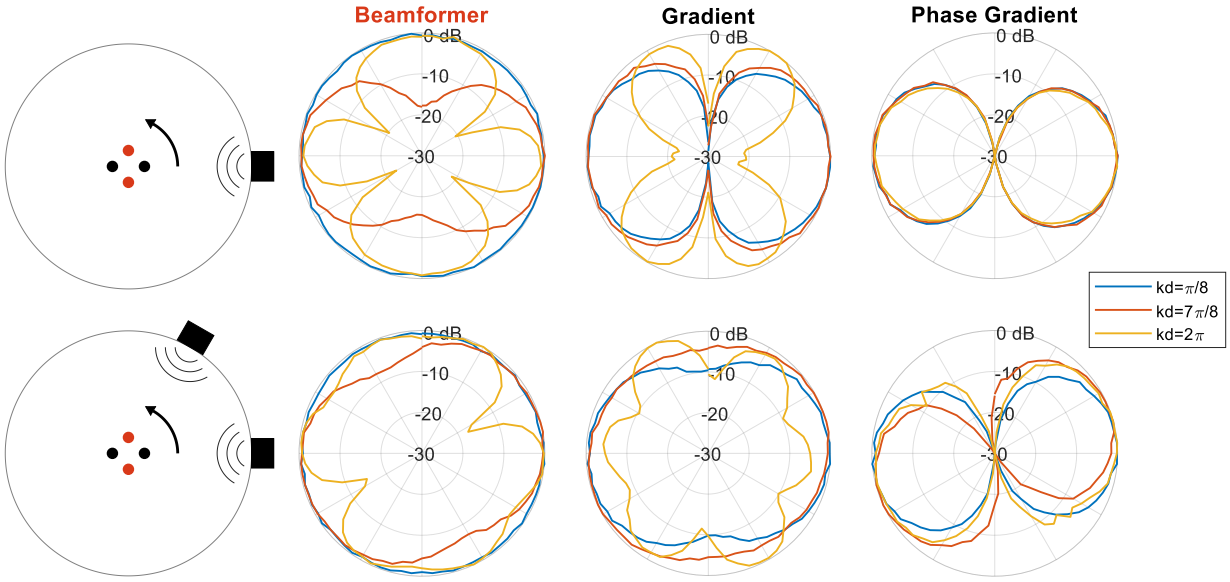

Figure 5.3. Top: Measured, two-microphone array response using a single loudspeaker at $kd = \pi/8, 7\pi/8,$ *and* 2π *using different processing methods: beamforming, traditional gradient sensing, and phase-gradient sensing. The gradient and phase gradient sensors were oriented such that at* $\theta = 0°$ *the two microphones (black dots) were in line with the source, whereas the beamformer requires the source be broadside the microphones (red dots). The microphone separation,* d*, and source distance in the schematic is not to scale. Bottom: Same for two loudspeakers separated by 60 degrees.*

To compare the methods' ability to resolve a single source, beamforming, traditional gradient sensing, and phase-gradient sensing are compared for the single loudspeaker experiment. While the first two method have erroneous sidelobes at higher frequencies (e.g., $kd = 2\pi$), the phase-gradient estimate of the directional pressure in Eq. (5.7) does not; the phase-gradient method shows a successful $\cos^2\theta$ array response up to the spatial Nyquist frequency ($kd = \pi$) and beyond when phase gradients can be properly unwrapped. As opposed to the other methods, this phase-gradient method yields consistent results over the entire frequency range where the microphones are receiving sufficiently coherent signals.

A beamformer involves time delays to steer the array,[57] although in the broadside case investigated here the time delays are zero and the signals are simply added. The broadside beamformer responds nearly omnidirectionally at low frequencies. At high frequencies the pattern becomes more directional, although grating lobes appear above the spatial Nyquist frequency of $kd = \pi$. Additional microphones make beamforming more effective at high frequencies, but the response still varies with frequency, and is nearly omnidirectional at low frequencies (small kd).

A traditional gradient sensor adds pressure signals together multiplied by finite-difference coefficients. In this two-microphone case, one microphone signal is subtracted from the other. This produces a $\cos\theta$ response for low frequencies.[49] However, at frequencies approaching and above the spatial Nyquist frequency ($kd = \pi$), finite-difference errors cause changes in the array response.

To test the methods' behavior in the presence of multiple sources, the experiment was repeated with two incoherent loudspeakers spaced $60°$ apart, and the results are shown in the bottom row of Fig. 3. None of the two-microphone methods resolve the individual sources. However, the peak response of the phase-gradient method is aimed between the two sources with a well-defined $\cos^2\theta$ pattern, clearly indicating the direction of the group of sources. The response angle at each frequency depends on the relative source amplitudes. The response of the beamformer and traditional gradient sensor have no strong peaks or nulls, resulting in an inconclusive estimate of the location of the group of sources.

In addition to the results above, the array response of the phase-gradient method can be increased by raising the power on the directivity factor, as in Eq. (5.10). Higher-order estimates calculated from the single-loudspeaker experiment are shown in Fig, 4(a), which matches the theoretical pattern shown in Fig. 2(a). Experimental noise causes the directivity factor to be slightly

higher than 1 when pointed at the source, a small error that is magnified by raising the directivity factor to higher orders. Figure 4(b) shows the experimental response of a unidirectional sensor of various orders [Eq. (5.11)], which can be compared with the theoretical response in Fig. 2(b). The response of the two-dimensional, four-microphone array is displayed in Figure 4(c) and obtained by computationally steering the unidirectional sensor in Eq. (5.12) without rotating the array.

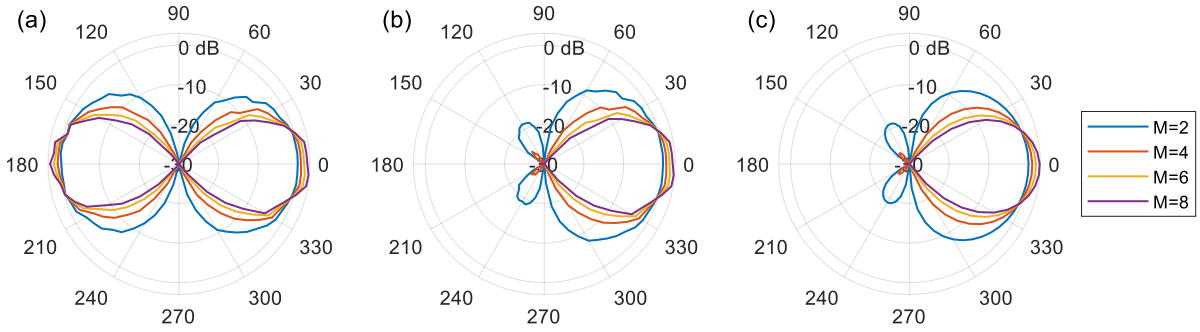

Figure 5.4. Measured, single-loudspeaker array response for phase-gradient method of order $M = 2$, 4, 6, and 8 for (a) a two-microphone bidirectional sensor, (b) a two-microphone unidirectional sensor obtained from rotating the array, and (c) a computationally-steered two-dimensional, unidirectional sensor, using a single measurement with the loudspeaker at 60 degrees from the x-axis of the 4-microphone array. All data shown is for 200 Hz, which in this case is $kd = 0.37$.

5.4 Conclusion

The phase-gradient method for directional pressure sensing explained in this letter avoids high-frequency, finite-difference error present in other methods. This approach allows for the creation of a two-microphone, frequency-domain array response with an arbitrary directivity order that is accurate up to the spatial Nyquist frequency. For broadband sources and with proper unwrapping, accuracy can be extended up to the limit of inter-microphone coherence.

Conventional gradient-based sensors have the advantage of returning signals in the time domain, allowing for the creation of live filtering such as in a cardioid microphone. However, the array responses of these microphones break down at higher frequencies due to finite-difference errors. Some finite-difference error is avoided by using particle velocity sensors, as done by de Bree and Wind.[53] However, these sensors can be sensitive to wind noise, complicating outdoor

measurements.[36] With sufficient distance between microphones, or with a phase-matching calibration, the low-frequency accuracy of microphone arrays can be made sufficient for most applications.

An additive beamformer avoids the finite-difference errors present in gradient microphones; however, the array response changes with frequency. At low frequencies, the response is nearly omnidirectional, whereas at high frequencies the directivity is much narrower but grating lobes appear. Beamforming can be used as a time-domain filter, but for use with intensity probes, the dimensions are too small and the microphone count is too low for the beamforming to be effective over most frequencies of interest. These comparisons indicate that phase gradient-based directional sensing is more effective for highly directional frequency-domain pressure sensing using a small number of microphones.

A primary drawback of the phase-gradient method for directional pressure is its limitation to the frequency domain. However, the possibility exists to use the frequency-dependent phase gradient to inform a time-domain filter for stationary systems. By using the phase gradient, the average direction of incoming sound at each frequency could be determined, which could then be used to filter the signal in the time domain. This filtering could either be done in blocks for recorded data or using an adaptive filter in real-time. Source discrimination would be possible up to the spatial Nyquist frequency. The robustness of this approach has yet to be determined.

Chapter 6

Conclusion

6.1 Conclusions

In determining the efficacy of the PAGE method for energy-based quantity estimation, it is vital to understand both the advantages and limitations of the method. This thesis furthers that objective through theoretical development, experimental verification, and extension of the PAGE formulation to additional quantities and applications.

Comparison of PAGE and traditional bias errors for two- and three-microphone probes shows bandwidth extension as a primary advantage of the PAGE method, removing high-frequency error when unwrapping is properly applied. This allows for the creation of probes with large microphone separation for improved low-frequency accuracy without losing high-frequency bandwidth. The addition of a center microphone removes the need to estimate center pressure by averaging, reducing near-field error. Therefore, the ideal method for one-dimensional active intensity estimation is three-microphone PAGE, with zero near-field or high-frequency error in a monopole field. However, specific acoustic impedance is best estimated using two-microphone PAGE. These results were verified experimentally.

With two microphones, PAGE and traditional estimates of reactive intensity are exactly the same, and the addition of a center microphone does little to reduce error in the near-field, the area where reactive intensity is the strongest and of greatest interest. A method for using additional microphones and higher-order derivatives was developed, and error reduction was shown

numerically. Although the PAGE method performs well in propagating fields, higher-order PAGE is out-performed in a standing wave field by a higher-order traditional method.

In extending the applications of the PAGE method, a method was developed for directional pressure sensing based on the phase gradient. Although limited to the frequency domain, use of the phase gradient extends the method's bandwidth over that of traditional methods, enabling accuracy up to the spatial Nyquist frequency and beyond when unwrapping is possible. Additionally, the phase gradient acts as a directivity factor, and can be modified to produce higher-order bidirectional and unidirectional responses using two microphones, as well as steerable responses using multi-dimensional arrays. These responses were experimentally verified.

6.2 Future Work

Although the current work characterizes the PAGE method for many relevant uses, the research was limited to ideal analytical fields and experimental verification in a nearly ideal anechoic environment. Mylan Cook is performing concurrent work in exploring behavior of the PAGE method in the presence of noise. Initial results indicate that the PAGE method is sensitive to the injection of uncorrelated noise whereas the traditional method is not. To obtain more accurate gradient estimates, especially in the presence of noise, a method for obtaining a coherence-weighted gradient estimate is under development. For an overdetermined microphone array containing more microphones than is strictly necessary to estimate a gradient, the least-squares gradient fit can utilize frequency-dependent coherence weights for each microphone pair to reduce the influence of microphones with poor signal.

Future work may synthesize the research presented in this thesis and the research done by Cook. The behavior of PAGE reactive intensity and directional pressure in the presence of noise can be explored. The higher-order method presented in Chapter 4 could be combined with the

coherence-weighted gradient fit, such that the gradient estimation would be neither fully determined as in the higher-method, nor strictly first-order as in the coherence-weighted method. In this way, a balance can be found between accurate higher-order modeling of the field and the rejection of sensors with poor signal. Current knowledge of the performance of the PAGE method in various applications and in the presence of noise could inform a thorough analysis of optimal probe design. Furthermore, work by Succo[30] could help incorporate the treatment of narrowband sources in these studies.

Further applications of the PAGE method may include further development of directional pressure. Applications for the directional pressure may be investigated, including potential modification of a real-time localization system developed by Young[26] to use directional pressure rather than active intensity. The directional pressure sensor developed in Chapter 5 is currently limited to the frequency domain, preventing use of the method for obtaining a filtered time-domain signal for potential applications. However, development of a time-domain method may be the subject of further study.

The possibility exists to use the phase gradient to inform a time-domain filter that can filter sources by direction. Taking the inverse Fourier transform of Eq. (5.10) shows that the time-domain directional pressure can be obtained by filtering the time-domain pressure of a single microphone. The filter is represented in the frequency domain as $(\partial\phi/\partial x)^M/k^M$, where M is the arbitrarily-chosen filter order. This filter is applied either by multiplication in the frequency domain before the inverse Fourier transform, or by convolution in the time domain. Effectively, this scales the magnitude at each frequency dependent on the direction of the phase gradient, creating a spatially-filtered time-domain signal sensitive to a particular direction. By using the phase gradient, the method is accurate up to the spatial Nyquist frequency for single or multiple

sources, and can be extended higher when unwrapping is possible. It will be important to investigate appropriate strategies for dealing with noise in the phase of the transfer function, as unwanted noise in the filter could corrupt the output signal. If a robust form of this method could be developed, it would be useful to obtain block-processed time-domain signals. Additionally, the phase gradient could be used to inform an adaptive filter that could be used for live audio with minimal lag.

Further analytical development of the PAGE method for energy-based quantity estimation may be possible. The directional pressure method discussed in Chapter 5 estimates pressure from a particle velocity gradient, similar to the pressure estimate obtained by a $\boldsymbol{u}$-$\boldsymbol{u}$ intensity probe.[52] This formulation for pressure could be incorporated into a $\boldsymbol{u}$-$\boldsymbol{u}$ form of the PAGE method. Also, the PAGE expressions for energy-based quantities could be extended to the time domain. Combination of an oscillating signal with its Hilbert transform creates an "envelope,"[14,63] a process that could be performed on the pressure to obtain a time-domain pressure amplitude, P, for use in instantaneous PAGE active and reactive intensity estimates. The phase gradient term, $\nabla\phi$, in the active intensity expression could be expressed as a time-domain filter using an inverse Fourier transform, as explained above for directional pressure.

In addition to the gradient-based directional sensing discussed in Chapter 5, the PAGE method could be applied to beamforming-based methods of directional sensing. This could include particle velocity beamformers, such as the one introduced by Gur.[64] This beamformer relies on particle velocity sensors and spatial derivatives of the particle velocity to obtain a highly-directive response with a small aperture. Replacing the particle velocity sensors with a microphone array and using principles of the PAGE method to obtain particle velocity derivatives may extend the

bandwidth of this method. Additionally, using microphones in place of particle velocity sensors would make the beamformer more robust for outdoor measurements.[36]

Appendix

A Implementation

The codes used to create the plots in this thesis are made available for members of the BYU Acoustics Research Group at https://pulsar.byu.edu/acoustics, and on the acoustics gamma drive. The main codes that create the plots for each chapter are Ch2_Plots.m, Ch3_Plots.m, Ch4_Plot2.m, Ch4_Plot3.m, and Ch5_Plots.m. JASA_2_Mic_Plots.m produces modified versions of the plots in Chapter 2 that were used in the article published in the *Journal of the Acoustical Society of America*.[32]

The repository also contains all dependent code for PAGE processing and plotting. This includes PAGE_func.m, which applies PAGE processing to given measured or simulated data. TRAD_func.m does the same for traditional processing, while PAGE_func_HO.m and TRAD_func_HO.m perform higher-order PAGE and higher-order traditional processing, respectively. The PAGE processing functions rely on unwrap_func.m to perform various unwrapping options, including the coherence-based unwrapping developed by Cook.[29]

Ch3_ProcessData.m prepares the Chapter 3 data, creating an output structure file needed by Ch3_Plots.m. The code relies on spectra.m, which loads the data for processing.

The folder Plot Tools contains code used for plotting. The codes with names beginning with ColormapPlot produce the color plots with either 1, 2, or 6 subplots, relying on fancyContours2.m for the plot creation and pcold2hot_generator.m for the colormap. The line plots are made by plotErrorM.m (magnitude only) and plotErrorPM.m (phase and magnitude). Export_fig is used to create high resolution TIFF images. The latest version of export_fig should be downloaded from https://github.com/altmany/export_fig. For export_fig to work with modern

versions of MATLAB, Ghostscript needs to be installed. Refer to the online documentation for export_fig for more information.

B Data

Three sets of data were used for plots in this thesis, all of which can be found on the acoustics gamma drive at Students\Joseph Lawrence\Thesis\Thesis Data. The first is 13OctBBSmall_Speaker, which was used for the experimental bias errors in Figs. 3.2, 3.3 and 3.4 in Chapter 3. Each scan was at a different distance from the probe, starting close to the probe and moved away in increments as given by the grid in Ch3_ProcessData.m. Channel 0 is the center microphone, Channel 1 is closest to the source, and Channel 2 is farthest. The outer two microphones were used for the two-microphone bias errors.

The other two data sets, 2Feb2D and 2Feb2D2Speaker were used for the measured array responses shown in Figs. 5.3 and 5.4 in Chapter 5. For both sets, the turntable was rotated 5 degrees for each scan, with the probe configuration given in Ch5_Plots.m.

Bibliography

1. R. Hickling, and A. W. Brown. "Determining the direction to a sound source in air using vector sound-intensity probes." J. Acoust. Soc. Am. **129**, 219–224 (2011).

2. Jacobsen, F., and Liu, Y. "Near field acoustic holography with particle velocity transducers," J. Acoust. Soc. Am. **118**, 3139–3144 (2005).

3. M. C. Harris, J. D. Blotter, and S. D. Sommerfeldt. "Obtaining the complex pressure field at the hologram surface for use in near-field acoustical holography when pressure and in-plane velocities are measured." J. Acoust. Soc. Am. **119**, 808–816 (2006).

4. Williams, E. G. *Fourier acoustics: sound radiation and nearfield acoustical holography* (Academic press, 1999).

5. Hickling, R., Lee, P., and Wei, W. "Investigation of integration accuracy of sound-power measurement using an automated sound-intensity system," Appl. Acoust. **50**, 125–140 (1997).

6. ISO 15186-1:2003. Acoustics - Measurement of Sound Insulation in Buildings and of Building Elements Using Sound Intensity - Part 1: Field Measurements (International Organization for Standardization, Geneva, Switzerland, 2003).

7. ISO 9614-3:2002. Acoustics - Determination of sound power levels of noise sources using sound intensity - Part 3: Precision Method for Measurement by Scanning (International Organization for Standardization, Geneva, Switzerland, 2002).

8. F. J. Fahy, "Measurement of acoustic intensity using the cross-spectral density of two microphone signals," J. Acoust. Soc. Am. **62**, 1057–1059 (1977).

9. F. J. Fahy, "A technique for measuring sound intensity with a sound level meter," Noise Control Eng. **9**, 155–162 (1977).

10. J. Y. Chung, "Cross-spectral method of measuring acoustic intensity without error caused by instrument phase mismatch," J. Acoust. Soc. Am. **64**, 1613–1616 (1978).

11. F. J. Fahy, *Sound Intensity* (Spon, London, 1995), pp. 1–295

12. B. S. Cazzolato and C. H. Hansen, "Errors arising from three-dimensional energy density sensing in one-dimensional sound fields," J. Sound Vib. **236**, 375–400 (2000).

13. J.-C. Pascal and J.-F. Li, “A systematic method to obtain 3D finite-difference formulations for acoustic intensity and other energy quantities,” J. Sound Vib. **310**, 1093–1111 (2008).

14. F. Jacobsen, "A note on instantaneous and time-averaged active and reactive sound intensity." J. Sound Vib. **147**, 489–496 (1991).

15. J. Y. Chung and D. A. Blaser, "Transfer function method of measuring acoustic intensity in a duct system with flow." J. Acoust. Soc. Am. **68**, 1570–1577 (1980).

16. J. Y. Chung and D. A. Blaser, "Transfer function method of measuring in-duct acoustic properties. II. Experiment." J. Acoust. Soc. Am. **68**, 914–921 (1980).

17. J. F. Allard and P. Delage, "Free field measurements of absorption coefficients on square panels of absorbing materials." J. Sound Vib. **101**, 161–170 (1985).

18. Y. Champoux, J. Nicolas, and J. F. Allard, "Measurement of acoustic impedance in a free field at low frequencies." J. Sound Vib. **125**, 313–323 (1988).

19. J. K. Thompson, and D. R. Tree, "Finite-difference approximation errors in acoustic intensity measurements," J. Sound Vib. **75**, 229–238 (1981).

20. Y. Champoux and A. L'espérance. "Numerical evaluation of errors associated with the measurement of acoustic impedance in a free field using two microphones and a spectrum analyzer." J. Acoust. Soc. Am. **84**, 30–38 (1988).

21. D. C. Thomas, B. Y. Christensen, and K. L. Gee, "Phase and amplitude gradient method for the estimation of acoustic vector quantities." J. Acoust. Soc. Am. **137**, 3366–3376 (2015).

22. D. K. Torrie, E. B. Whiting, K. L. Gee, T. B. Neilsen, and S. D. Sommerfeldt, "Initial laboratory experiments to validate a phase and amplitude gradient estimator method for the calculation of acoustic intensity," Proc. Mtgs. Acoust. **23**, 030005 (2017).

23. K. L. Gee, T. B. Neilsen, S. D. Sommerfeldt, M. Akamine, and K. Okamoto, "Experimental validation of acoustic intensity bandwidth extension by phase unwrapping," J. Acoust. Soc. Am. **141**, EL357–EL362 (2017).

24. T. A. Stout, K. L. Gee, T. B. Neilsen, A. T. Wall, and M. M. James, "Source characterization of full-scale jet noise using acoustic intensity." Noise Control Eng. J. **63**, 522–536 (2015).

25. K. L. Gee, E. B. Whiting, T. B. Neilsen, M. M. James, and A. R. Salton, "Development of a near-field intensity measurement capability for static rocket firings," Trans. Jpn. Soc. Aeronaut. Space Sci. **14**, PO_2_9–PO_2_15 (2016).

26. J. G. Young, J. S. Lawrence, and K. L. Gee. "Real-time source localization using phase and amplitude gradient estimator for acoustic intensity," J. Acoust. Soc. Am. **143**, 1837–1837 (2018).

27. M. T. Rose, R. D. Rasband, K. L. Gee, and S. D. Sommerfeldt, "Comparison of multi-microphone probes and estimation methods for pressure-based acoustic intensity." Proc. Mtgs. Acoust. **26**, 030004 (2016).

28. E. B. Whiting, "Energy Quantity Estimation in Radiated Acoustic Fields." Master's thesis, Brigham Young University, Provo, UT, 2016.

29. M. R. Cook, K. L. Gee, S. D. Sommerfeldt, and T. B. Neilsen "Coherence-based phase unwrapping for broadband acoustic signals" Proc. Mtgs. Acoust. **30**, 055005 (2017).

30. K. F. Succo, "Acoustic Intensity of Narrowband Signals in Free-Field Environments." Master's thesis, Brigham Young University, Provo, UT, 2017.

31. C. B. Goates, B. M. Harker, T. B. Neilsen, and K. L. Gee, "Extending the bandwidth of an acoustic beamforming array using phase unwrapping and array interpolation." J. Acoust. Soc. Am. **141**, EL407–EL412 (2017).

32. E. B. Whiting, J. S. Lawrence, K. L. Gee, T. B. Neilsen, and S. D. Sommerfeldt, "Bias error analysis for phase and amplitude gradient estimation of acoustic intensity and specific acoustic impedance," J. Acoust. Soc. Am. **142**, 2208–2218 (2017).

33. J. S. Lawrence, E. B. Whiting, K. L. Gee, R. D. Rasband, T. B. Neilsen, and S. D. Sommerfeldt, "Three-microphone probe bias errors for acoustic intensity and specific acoustic impedance." J. Acoust. Soc. Am. **143**, EL81–EL86 (2018).

34. J. S. Lawrence, K. L. Gee, T. B. Neilsen, and S. D. Sommerfeldt, "Higher-order estimation of active and reactive acoustic intensity." Proc. Mtgs. Acoust. **30**, 055004 (2017).

35. F. Jacobsen and H. E. de Bree, "A comparison of two different sound intensity measurement principles." J. Acoust. Soc. Am. **118**, 1510–1517 (2005).

36. W. F. Druyvesteyn and H. E. De Bree, "A novel sound intensity probe comparison with the pair of pressure microphones intensity probe." J. Audio Eng. Soc. **48**, 49–56 (2000).

37. J. H. Giraud, K. L. Gee, and J. E. Ellsworth, "Acoustic temperature measurement in a rocket noise field." J. Acoust. Soc. Am. **127**, EL179–EL184 (2010).

38. G. Pavić, "Measurement of sound intensity," J. Sound Vibr. **51**, 533–545 (1977).

39. S. J. Elliott, "Errors in acoustic intensity measurements," J. Sound Vib. **78**, 439–443 (1981).

40. F. Jacobsen, V. Cutanda, and P. M. Juhl, "A numerical and experimental investigation of the performance of sound intensity probes at high frequencies," J. Acoust. Soc. Am. **103**, 953–961 (1998).

41. C. P. Wiederhold, K. L. Gee, J. D. Blotter, and S. D. Sommerfeldt, "Comparison of methods for processing acoustic intensity from orthogonal multimicrophone probes," J. Acoust. Soc. Am. **131**, 2841–2852 (2012).

42. C. P. Wiederhold, K. L. Gee, J. D. Blotter, S. D. Sommerfeldt, and J. H. Giraud, "Comparison of multimicrophone probe design and processing methods in measuring acoustic intensity," J. Acoust. Soc. Am. **135**, 2797–2807 (2014).

43. IEC 1043:1993, “Electroacoustics—Instruments for the measurement of sound intensity—Measurement with pairs of pressure sensing microphones” (International Electrotechnical Commission, Geneva, Switzerland, 1993).

44. ANSI/ASA S1.9-1996, Instruments for the Measurement of Sound Intensity (Acoustical Society of America, Melville, NY, 1996).

45. J. A. Mann III, J. Tichy, and A. J. Romano, "Instantaneous and time-averaged energy transfer in acoustic fields." J. Acoust. Soc. Am. **82**, 17–30 (1987).

46. F. P. Mechel, "New method of impedance measurement." Proceedings of the 6th ICA, H217–H220 (1968).

47. K. L. Gee, M. Akamine, K. Okamoto, T. B. Neilsen, M. Cook, S. Tsutsumi, S. Teramoto, and T. Okuuki, "Characterization of supersonic laboratory-scale jet noise with vector acoustic intensity," in 23rd AIAA/CEAS Aeroacoustics Conference, AIAA Paper 2017–3519 (2017).

48. P. S. Jensen, "Finite difference techniques for variable grids," Comput. Struct. **2**, 17–29 (1972).

49. H. F. Olson, "Gradient Microphones," J. Acoust. Soc. Am. **17**, 192 (1946).

50. B. A. Cray, V. M. Evora, and A. H. Nuttall, "Highly directional acoustic receivers," J. Acoust. Soc. Am. **113**, 1526 (2003).

51. E. De Sena, H. Hacihabiboglu, and Z. Cvetkovic, "On the design and implementation of higher order differential microphones," IEEE Trans. Audio Speech Lang. Process. **20**, 162-174 (2012).

52. K. J. Bastyr, G. C. Lauchle, and J. A. McConnell, "Development of a velocity gradient underwater acoustic intensity sensor," J. Acoust. Soc. Am. **106**, 3178-3188 (1999).

53. H. E. de Bree and J. Wind, "A particle velocity gradient beam forming system," J. Acoust. Soc. Am. **127**, 1820 (2010).

54. S. Yu, D. F. Comesaña, G. C. Pousa, Y. Yang, and L. Xu, "Unidirectional acoustic probe based on the particle velocity gradient," J. Acoust. Soc. Am. **139**, EL179 (2016).

55. G. M. Sessler and J. E. West, "Second-order gradient unidirectional microphones utilizing an electret transducer," J. Acoust. Soc. Am. **58**, 273-278 (1975).

56. J. C. Chen, K. Yao, and R. E. Hudson, "Source localization and beamforming," IEEE Signal Proc. Mag. **19**(2), 30–39 (2002).

57. B. D. Van Veen and K. M. Buckley, "Beamforming: A versatile approach to spatial filtering," IEEE ASSP Mag. **5**, 4–24 (1988).

58. A. Nehorai and E. Paldi "Acoustic vector-sensor array processing," IEEE Trans. Signal Process. **42**, 2481–2491 (1994).

59. D. J. Schmidlin "Directionality of generalized acoustic sensors of arbitrary order," J. Acoust. Soc. Am. **121**, 3569–3578 (2007).

60. M. E. Lockwood and D. L. Jones, "Beamformer performance with acoustic vector sensors in air," J. Acoust. Soc. Am. **119**, 608–619 (2006).

61. Y. Song and K. T. Wong, "Azimuth-elevation direction finding using a microphone and three orthogonal velocity sensors as a non-collocated subarray." J. Acoust. Soc. Am. **133**, 1987-1995 (2013).

62. E. Gorman, S. Bunkley, J. E. Ball, and A. Netchaev, "Direction of arrival estimation for conformal arrays on real-world impulsive acoustic signals," Proc. Mtgs. Acoust. **31**, 055003 (2018).

63. N. Thrane, J. Wismer, H. Konstantin-Hansen, and S. Gade, "Practical use of the Hilbert transform," Bruel & Kjaer Application Note, BO 0437-11 (1999).

64. B. Gur, "Particle velocity gradient based acoustic mode beamforming for short linear vector sensor arrays," J. Acoust. Soc. Am. **135**, 3463–3473 (2014).